

FINAL REPORT

Graduation Thesis

Modelling soil cutting processes in a modular structured program (Dynamic soil cutting)



This page is left blank intentionally

Modelling soil cutting processes in a modular structured program (Dynamic soil cutting)

Author:

R. Hasan

Educational institution:	HZ University of Applied Sciences
Student number:	0078501
Company:	Damen Dredging Equipment
Location of company:	Nijkerk
Study program:	Civil Engineering
University supervisor:	Marco Gatto
In-company supervisor:	Mark Winkelman
Graduation project duration:	01/02/2022 – 17/06/2022

Preface

The last 5 months I was able to work on my Bachelors thesis in the company Damen Dredging Equipment. I want to thank Damen Dredging Equipment and Frank Bosman for giving me the opportunity to work on modelling soil cutting processes in a modular structured program.

This report is meant for whom is interested in soil cutting, dredge machinery. As well as whom is interested in rotary cutting movement of the soil.

I would like to thank my company supervisor Mark Winkelman for all his supervision and all the knowledge that he shared with me. I also want to thank all the colleagues from the Research Development and Innovation the department whom helped me during this thesis and gave me a lot of inside knowledge of the dredging industry.

Rahaf Hasan

Friday 17th June, 2022

Table of Contents

List of Figures	4
Introduction	6
Host Organization	6
Background.....	6
Problem Statement.....	8
Research Questions	9
Research Objective	10
Research Outline.....	10
Theoretical Frame Work.....	11
Requirements for the MATLAB module:	19
Pre-conditions:.....	19
Methodology	20
Results	24
Parameter defining experiments:.....	24
MATLAB module:	26
Soil cutting experiment.....	29
Discussion	30
Conclusion and recommendations	31
References.....	32
Appendices	34
Appendix A.....	34
Appendix B.....	34
Appendix C.....	35

List of Figures

Figure 1, Cutter Suction Dredger (Association of Dredging Companies, n.d.)	7
Figure 2, Adapter system (left), teeth range with adapter (top), teeth range direct on arm (bottom) (Winkelman, n.d.)	8
Figure 3, Main cutter head components from DDE	8
Figure 4, Cutting mechanisms (Lee et al., n.d.)	8
Figure 5, The rotary trajectory of each teeth	9
Figure 6, Cutter head representation of CSD	9
Figure 7, The rotary trajectory of each teeth (front view)	9
Figure 8, Particle size distribution curves (Budhu, 2010)	11
Figure 9, The forces on the layer of soil cut (left) and the forces acting on the blade/teeth (right) (S. Miedema, 2015)	13
Figure 10, The flow lines (S. Miedema, 2015)	14
Figure 11, 3D cutting process (S. Miedema, 2015)	18
Figure 12, Rotary sand cutting experiment	20
Figure 13, Sieve stack	21
Figure 14, Density test	21
Figure 15, Measurement of the lid surface	22
Figure 16, placing ovals in PowerPoint to know the scaling factor	22
Figure 17, Using PowerPoint to find the scaling factor	23
Figure 18, particle size distribution curve obtained from the sieve analysis	24
Figure 19, Permeability values from tests and experiments	25
Figure 20, Structure of the MATLAB script	26
Figure 21, The original normal force	27
Figure 22, the wedge length has surpassed the blade length	28
Figure 23, the wedge has reached the blade length	28
Figure 24, beginning of the wedge formation	28
Figure 25, The improved normal forces, with the addition of the gravitational force, the centrifugal force, and the inertial force	28
Figure 26, the original and improved normal forces	29
Figure 27, Torque from the forces on the blade (orange) and from the weight of the bottles (blue)	29
Figure 28, cutting sand with a wedge	30

Nomenclature

τ	Shear stress	pa
c	Cohesion	pa
φ	Internal friction angle	rad
δ	Soil/steel interface friction angle	rad
α	Cutting angle blade	rad
β	Shear angle	rad
σ	Normal stress	pa
N_1	Normal force on the shear zone	N
N_2	Normal force on the blade	N
w	Width of the blade	m
W_1	Pore pressure force on the shear zone	N
W_2	Pore pressure force on the blade	N
ε	Dilatation	-
n_{cv}	Constant volume of porosity	-
n_i	Initial porosity	-
h_b	Height of the blade	m
h_i	Thickness of the cut layer	m
s_1	Flowline 1	m
s_2	Flowline 2	m
s_3	Flowline 3	m
s_4	Flowline 4	m
L_{max}	Variable length in the shear zone	m
L	Variable length	m
k_i	Initial permeability	m/s
k_m	Effective permeability	m/s
k_{max}	Maximum permeability	m/s
ρ_w	Density of water	Kg/m ³
ρ_s	Density of soil	Kg/m ³
g	gravity	m/s ²
v_c	Cutting velocity perpendicular to the edge of the blade	m/s
ν_1	kinematic viscosity	M ² /s
R_1	Resistance flow 1	s
R_2	Resistance flow 2	s
R_3	Resistance flow 3	s
R_4	Resistance flow 4	s
R_t	Total resistance flow	s
P_{1m}	Pore pressure in the shear plane	pa
P_{2m}	Pore pressure on the blade	pa
E_{nc}	Specific energy for non cavitating process	N/m ²
E_{ca}	Specific energy for cavitating process	N/m ²
c_1	Coefficient (non cavitating process)	-
a_1, a_2	Weight factors	-
d_1	Coefficient (cavitating process)	-
z	Water depth	m
k	permeability	m/s

Introduction

Host Organization

This project is being conducted at Damen Dredging Equipment which is one of the many Damen companies at the Research, development, and innovation (RD&I). “Damen Dredging Equipment is the Damen yard dedicated to the dredging industry. The yard specializes in the design, manufacture and supply of highly efficient dredging tools and services. An extensive standard range of powerful and robust dredgers is available, such as cutter suction dredgers, DOP dredgers, trailing pipe systems as well as a wide variety of dredging components such as dredge pumps. Like all Damen yards our vessels are built on stock and are ready for outfitting with various options” (*Damen Dredging Equipment - Damen, n.d.*).

Background

At the beginning of civilization, the transportation of goods was largely based on the depth of the oceans and inland waterways. Silting, which is a natural phenomenon that occurs when the water's content gets deposited over the seabed, can affect the navigation of ships. People were initially reluctant to deal with the issue due to the lack of equipment to remove siltation. Mills were first used for digging in ports during the 1570s. When the first models of mills were made, they were manually driven by hand (Wankhede, n.d.).

Prior to 1850, dredging and dredge contracting were mainly carried out by hand. This equipment was very simple and very basic. Many people looked for better equipment and solutions. During the middle ages, the Dutch contractors became skilled in hydraulic engineering. Due to the ongoing battle against the water in the lower regions of the rivers, they often used steam buckets. The initial designs of steam dredgers were not ideal for the Dutch soil. Eventually, the industry has become an important part of the Dutch economy (*DREDGING HISTORY, n.d.*). In 1867, a French engineer developed a suction dredger that was used to dredge the Suez Canal. It became widely used in the following decades (Wankhede, n.d.).

However, the question may arise as to what dredging and a dredger are. Dredging is the removal of sand, clay, or rock from water bodies, such as lake, rivers, sea, ...etc (*What Is Dredging?, n.d.*). As for a dredger, it is a ship or vessel that carries equipment that cuts and remove soil and mud from waterways. Some of the main drivers for dredging are:

- Increase of population, which in turn resulted in the need for land reclamation.
- World trade; due to the large increase of the trading and shipping business the need for larger and bigger ports and harbours construction to accommodate the ever increasing size of ships has arising.
- The need to maintain ports and harbours from sedimentation has called for dredging.
- Coastal protection; attributable to sea level rise and climate change, the demand to reinforce coastal defences has commenced (*Why Start Dredging? - Start Dredging, n.d.*).

There are two types of dredgers; mechanical dredgers, such as, bucket ladder dredger, backhoe dredger, and clam or grab dredger. Hydraulic dredgers, such as, cutter suction dredger, plain suction dredger, and the trailing suction hopper dredger.

The type of dredgers can also be identified according to their operation mechanism; stationary and non-stationary. Stationary dredgers are dredgers that are not propelled and stay in place when they are operational. On the other hand, non-stationary dredgers are seagoing or inland vessels that are usually self-propelled.

Cutter suction dredger, backhoe dredger, and dipper dredger are classified as stationary dredgers. While, trailing suction hopper dredger, and split hull dredgers are classified as non-stationary dredgers (VOUW, 2010b).

In this paper only the cutter suction dredger (CSD) and the cutting processes of the CSD is be discussed. The cutter suction dredger is called a stationary dredger because it is anchored during dredging. In reality, the CSD, and therefore the rotary cutter, swing in an arc around a fixed point. This point is maintained in a fixed position by means of anchors or a pile (spud) while the rotary cutter is moved back and forth with side cables. The rotary cutter therefore follows an arc-shaped path (Figure 1).

Attached to the CSD is the ladder, which at the end of it, a cutter head is mounted. The depth of the cutter head is controlled by the ladder winch. After the material is dredged, the soil is sucked into the suction nozzle through the pump. The dredged material is usually hydraulically transported using pipeline.

The CSD can dredge all type of materials such as, clay, sand, and rock, due to the cutting power that can range from 20 kW (Association of Dredging Companies, n.d.) and up to 44,180 kW (Spartacus cutter suction dredger) (*DEME Takes Delivery of 'Spartacus' - the Most Powerful and Innovative Cutter Suction Dredger in the World | DEME Group, n.d.*).

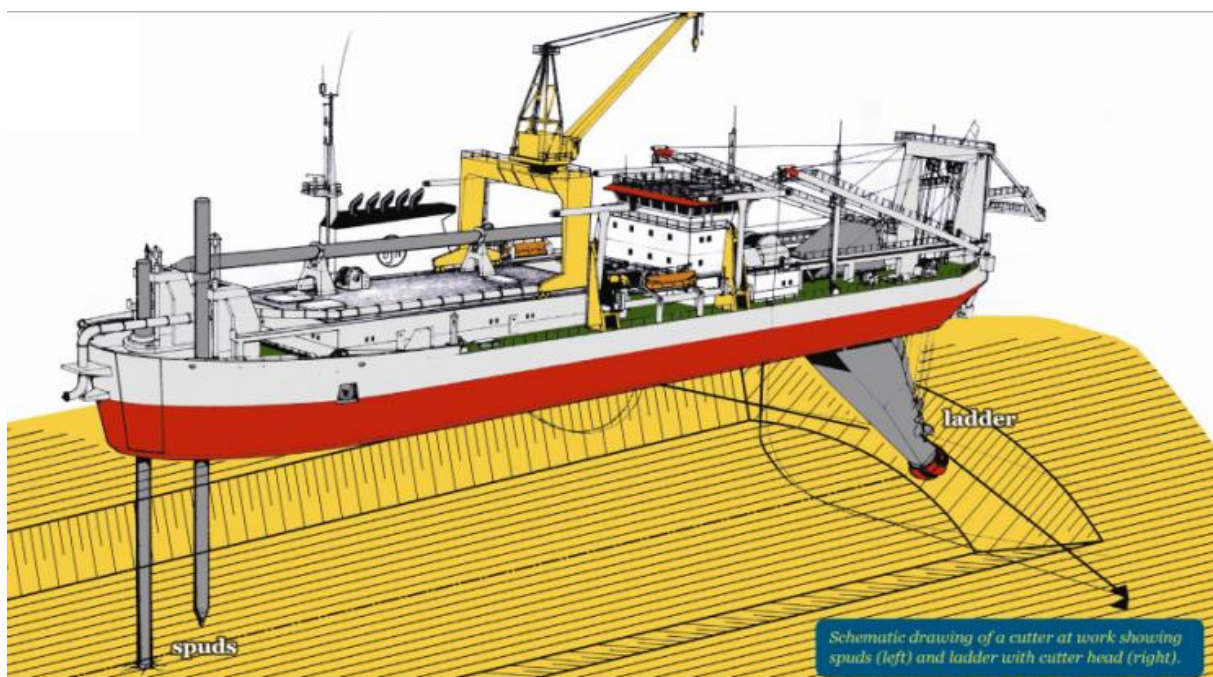


Figure 1, Cutter Suction Dredger (Association of Dredging Companies, n.d.)

The geometry of the cutting head and the type of teeth attached, depends on the type of soil that is being dredged. The different type of teeth that can be attached to the cutter head arm can be distinguished in Figure 3. (Winkelman, n.d.) states, the narrower teeth types should be used when hard soils are encountered and wider teeth should be selected for softer soils and for increased productivity. Although, it should be mentioned, the cutting depth of the wider teeth is less.

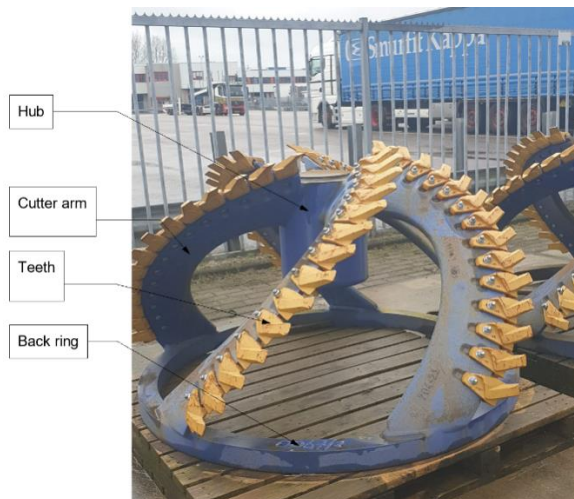


Figure 3, Main cutter head components from DDE

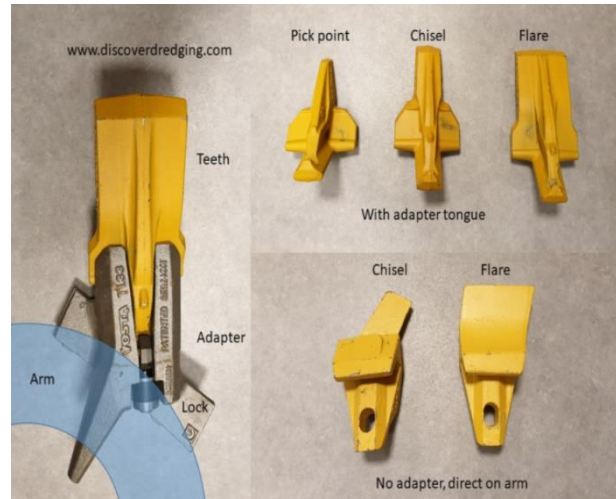


Figure 2, Adapter system (left), teeth range with adapter (top), teeth range direct on arm (bottom) (Winkelman, n.d.)

Depending on the teeth of the cutter head, the direction of cutting can be established; clockwise or anti-clockwise. In addition, if the cutter head's teeth are positioned to rotate anti-clockwise and it is operated in the same direction, then cutting process is called overcut. If it is operated in the opposite direction (clockwise) then it is called undercutting (Figure 4). Overcutting causes the less pull on the winches due to the reaction force created when the cut soil tugs the dredger along with it (Vlasblom, 2005). On the other hand, undercutting results in more forces on the winches and as such more effort is required to stabilize the dredger (VOUW, 2010a).

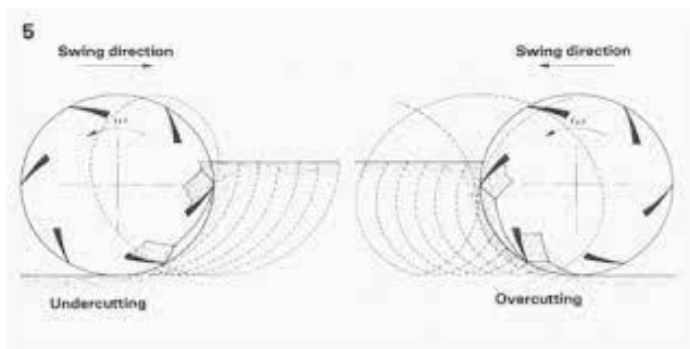


Figure 4, Cutting mechanisms (Lee et al., n.d.)

Problem Statement

The cutter suction dredger is one of the major products in Damen's portfolio. On the front a cutter is mounted. The cutting of soil by means of a cutter head is well known method of excavating sediments in the dredging industry. It involves a cutter head fitted with teeth that dig into the soil. There are many modules to describe the cutting process. However, most are based on cutting a blade along a straight line. In reality, the teeth are rotating around the cutter shaft and the cutting is along a curved trajectory with a varying cut height.

Currently, Damen is building a cutter design tool that is able to stimulate trajectories of the teeth. With the tool, staggering of the teeth can be checked and load variation can be evaluated for further design requirements for the rest of the dredge construction.

The tool is a MATLAB script that is able to provide the loads applied on the teeth of the cutter head during the rotary cutting motion of the teeth. A part of the MATLAB script regarding the kinetic movement of the teeth is already established (Figure 5, Figure 6, and Figure 7). From the kinetic MATLAB module, the teeth position, the cutting speed, the teeth angle, the teeth height, the

working depth, the thickness of the cut layer, ...etc are known. The parameters that are obtained from the kinetic module are used as input for the MATLAB module that is developed during this project, which calculates the cutting forces and the forces applied on the teeth.

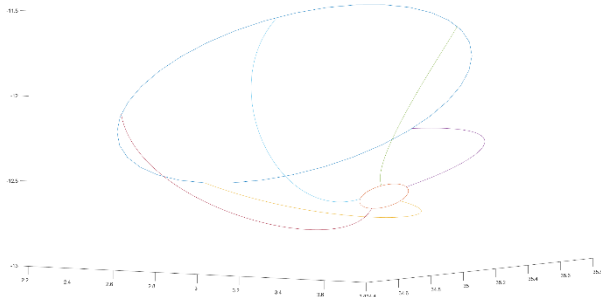


Figure 6, Cutter head representation of CSD

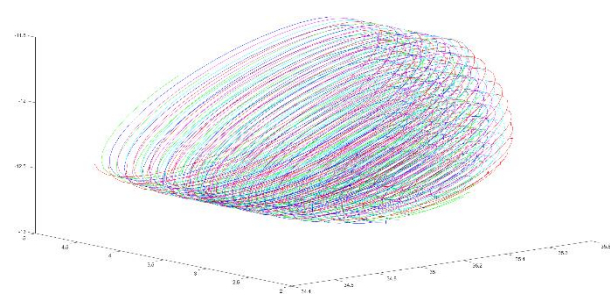


Figure 5, The rotary trajectory of each teeth

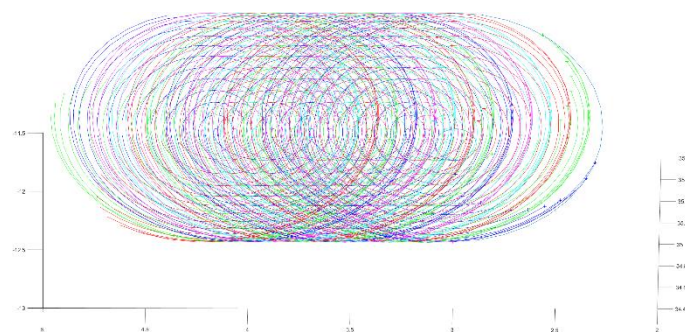


Figure 7, The rotary trajectory of each teeth (front view)

Currently, the cutting forces themselves are only roughly estimated by a Specific Cutting Energy assumption. Throughout literature, many assumptions are made about different parameters, the condition in which the cutting process is taking place, and in specific cases, some parameters are not even considered in the calculation process. This is usually done to simplify and provide results that can be verified through experiments or previous literature. One example of this would be, (S. Miedema, 2015) which provides extensive research and equations to calculate the cutting forces and the cutting energy. However, he calculate these forces based on the forces equilibrium principle, when in reality, the entire cutting process is constantly dynamic (This is explained in detail in the Theoretical Framework chapter).

As a result, Damen is looking for a more elaborate module that will calculate the expected cutting forces along the trajectory depending on the circumstances at each momentary position of the teeth there. Thus, in this project, the cutting forces of saturated sand is studied to gain the insight and knowledge required to create a MATLAB module that in principle should provide an outcome that takes into account the rotary trajectory of the cutting process.

Research Questions

What is the relation between the movement of cutter head's teeth of the CSD through the sediment and effort it takes?

From the main research question, sub-questions can be imposed to be able to obtain a good answer for the main question. These sub-questions are:

1. What function needs to be provided to be able to model the dynamic cutting of sand in MATLAB?
2. How will the parameters needed for the forces calculation be defined and obtained?
3. How will the results from the MATLAB module be verified?
4. What methods are going to be utilized to achieve the final objective?
5. How does the rotary trajectory differ from a straight trajectory?

Research Objective

The RD&I branch within the company Damen Dredging Equipment has established a MATLAB script that provide the kinetic movement of the teeth that are installed on the cutter head of the cutter suction dredger. In addition, the trajectory the teeth make when they are cutting the soil is already established. However, what is needed is a software module in MATLAB, that has to be plugged in the existing MATLAB script, for calculating the rotary dynamic cutting forces in sand. The result should be a module that can be called the main program of the cutter design tool. This project describes the module used, the framework for the module selection, and how the these have been implemented in the module.

A data string is given with the following parameters: velocity, angle, and cutting height. Then functions are created so that after inputting the aforementioned parameters, the cutting forces, the sliding force (the force of the materials sliding over the blade), ...etc, will be defined.

By creating this function in the MATLAB module, the rotary trajectory of the sand cutting should be able to provide a more accurate results than cutting along a straight line, as it closer to what occur in reality. In order to ensure that the results of the module are correct, tests are run on the module itself, along with an experiment that resembles the cutting process of one blade on a bed of water saturated sand. Eventually, a better understanding is needed of how the rotary movement of the teeth is affecting the loads applied on the blade and as such how much effort it will take to cut the soil.

Furthermore, the MATLAB tool that is developed during this project is structured to calculate the cutting forces to cut sand, which behave differently than other types of soils. However, if the module is successful, other tools similar to this one can be developed for other kind of soils.

Project Outline

The report comprises of 5 main chapters: theoretical framework, methodology, results, discussion, and conclusion chapter. In the theoretical frame work chapter, an evaluation of various other related research is conducted. The current knowledge is stated, therefore, narrowing the scope of the project, along with, establishing the focus of this study and providing an informative insight. Moreover, studying the similarities to this study and extract information that can be useful for this project. The methodology chapter follows the theoretical framework and describes the process to be taken to obtain, process, and the quantify the information in this study. Subsequent the methodology chapter, the results chapter, which showcases the results obtained from the MATLAB script and the experiments. After the results chapter comes the discussion chapter. This chapter discusses, reflect, and evaluate the results obtained. Lastly, the conclusion chapter summaries the discussion and states the main findings of the project, as well as, recommendations for future studies.

Theoretical Framework

In this chapter, all information found from literature regarding the cutting processes, the cutting forces, and the equilibrium of the cutting forces is discussed. However, in order to provide better understanding of the soil behaviour, the meaning of some parameters used in formulas, and why these specific parameters and formulas are used, some soil mechanics fundamentals is explained.

Particle size distribution and particle size distribution curve :

Particle size distribution is the separation of a soil sample into a variation of fractions based on their sizes. Rarely, is a soil sample that consists only of the same particle sizes. Generally, a soil sample is comprised of particles of many different sizes. The sizes of the particles can range from fine to coarse.

To obtain the particle size distribution a sieve analysis (described in Methodology) and a sedimentation analysis is usually performed. Particles with size less than 0.075 mm, carry charges on their surface and tend to cling to other particles. Therefore, to separate the smaller particles from the bigger ones, a wet sieve analysis is carried out, in which, the sample is washed through the 0.075mm sieve to remove the fine particles that are sticking to the bigger particles. Thereafter, the soil left in the 0.075mm sieve, is dried in an oven and a dry sieve analysis is then carried out. The fine particles that passed through the 0.075 mm sieve is used in a sedimentation analysis by utilizing the hydrometer method.

A graph (Figure 8) is plotted between percentage finer than D and diameter of the particle D. The graph's curve is called particle size distribution curve, it can also be called gradation curve (Budhu, 2010). While grading of the soil represent the distribution of particles in a soil mass. Soil properties can be estimated just from observing the gradation curve, for example, type of the soil and the gradation of the soil. A particle size distribution curve can represent a soil that is well graded, uniformly graded, and gap graded (S. Miedema, 2015). Well graded soil is a soil sample that has a good distribution of almost all particle's sizes, ranging from fine to coarse. On the other hand, uniformly graded soil or a poorly graded soil is a soil that has a deficiency or excess of certain particle sizes. There can also be another type of soil gradation, in which, some particle sizes are missing in between other sizes, this type is called gap graded soil.

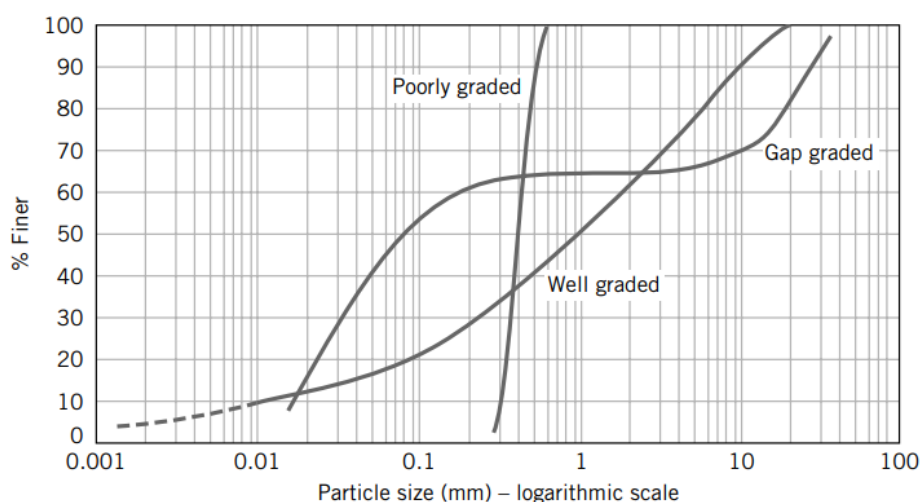


Figure 8, Particle size distribution curves (Budhu, 2010)

Density and relative density:

Density is mass per unit volume (Verruijt, 2001). The unite weight of the soil also gives information about it, such as, strength, and permeability.

Dilatation:

Dilation refers to an expansion or a change in the volume of a substance, which occurs when its shape is changed (S. Miedema, 2015). Dilatation can be calculated from the equation below:

$$\epsilon = \frac{dV}{V} = \frac{n_{cv} - n_i}{1 - n_{cv}} = \frac{dn}{1 - n_{cv}} \quad (1)$$

Permeability:

A soil mass is composed of small solid particles called soil grains. Those grain are arranged randomly and the empty space between the particles are called voids. This voids are interconnected and form a highly irregular tube like structures. When water is subjected to a pressure difference, the water will flow from the high to the low pressure through these voids. Depending on the type of voids and degree of irregularity of these tube structures, the ease of the water flow through the voids can be determined. Permeability is when the soil which allows a flow inside it. The easier the water flow through the voids the higher the permeability and vice versa (Purushothama, 2013).

Angles of repose, internal and external friction:

The stability of a sloping surface due to the presence of loose material is determined by the angle of repose. The angle of internal friction of a given soil is usually determined by analysing the graph of the shear stress and its normal effective stresses, where the shear failure happens. While, the external friction or the friction angle between a material and a soil medium can be expressed in degrees (S. Miedema, 2015). The values of the angle of external friction can be calculated using the table below.

20°	steel piles (NAVFAC)
0.67·φ-0.83·φ	USACE
20°	steel (Broms)
3/4·φ	concrete (Broms)
2/3·φ	timber (Broms)
2/3·φ	Lindeburg
2/3·φ	for concrete walls (Coulomb)

Table 1, External friction angle values (S. Miedema, 2015)

Shear strength and shear angle:

Soil mechanics refers to the degree of shear resistance that a soil can sustain. This resistance is caused by the interlocking of particles and the potential cementation or bonding at particle contacts. (S. Miedema, 2015) and (Verruijt, 2018) state that Coulomb law to calculate the shear stress is:

$$\tau = c + \sigma \cdot \tan(\varphi) \quad (2)$$

To determine the shear angle a function is created for it **Error! Reference source not found.**, based on the formula provided by (S. Miedema, 2015):

$$\beta = 61.29^\circ + 0.345 \cdot \frac{h_b}{h_i} - 0.3068 \cdot \alpha - 0.4736 \cdot \delta - 0.248 \cdot \phi \quad (3)$$

Now that the important soil mechanics parameters are discussed and explained. The forces that occur during saturated sand cutting according to literature is elaborated. Firstly, the processes that transpire when saturated sand is cut are clarified. Thenceforth, only the forces that are relative to this project are elucidated.

According to (S. Miedema, 2015), there are 6 types of failure mechanisms in relation to soil cutting. These failure mechanisms are: the curling type, the flow type, the tear type, the shear type, the chip type, and the crushed type (Appendix A). The failure mechanism for the cutting of saturated sand is the shear type. When cutting saturated sand the forces that can be distinguished are the pore vacuum pressure forces, external and internal friction angles. (S. Miedema, 2015), assumes that the failure lines are straight lines and a 2D plain strain cutting process for simplification.

During the cutting process, the volume of sand increases. This phenomenon is known as dilatancy. The change in the pore volume is caused by the shear in the sand. Water then will flow to the added pore volume. However, the water that is flowing to the pore volume endures a resistance, causing sub-pressures in the pore water in the sand (Zhao & Miedema, 2001). Due to the increased grain stresses, the required cutting forces increases as well. The rate at which the sand's volume is increased is proportional to the velocity at which the sand is cut. Saturated water vapor pressure and cavitation take place once the volume strain rate is high. An increase of the volume strain rate will not affect the pore pressure (Yasheng et al., 2006). However, since the increasing volume strain does not affect the pore pressure, it does not increase the cutting forces. The forces can still increase with the help of the inertia forces and the flow resistance (S. Miedema, 2015).

Conferring to (S. A. Miedema, n.d.), although the dilatancy phenomenon is not the only factor related to the cutting process, when low velocities occur, it has a major influence on the cutting process. This means that the contributions of the cohesion, adhesion, gravitation, and inertial forces can be neglected.

(S. Miedema, 2015) states that the equilibrium of the forces are:

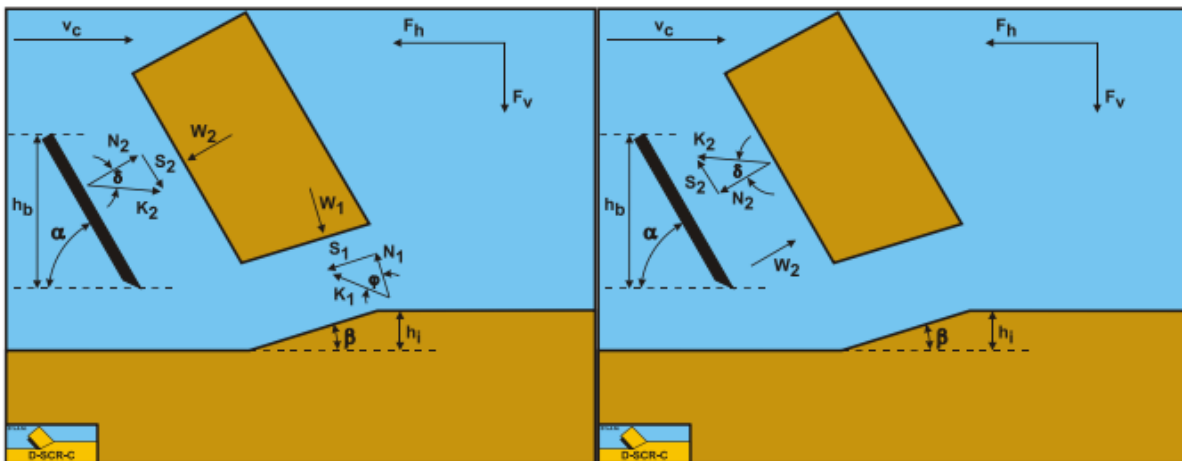


Figure 9, The forces on the layer of soil cut (left) and the forces acting on the blade/teeth (right) (S. Miedema, 2015).

Where:

1. N_1 is a normal force acting on the shear surface.
2. S_1 is a shear force as a result of the internal friction $N_1 \cdot \tan(\phi)$.

$$s_4 = (L_{max} - L) \cdot \theta_4 + 0.9 \cdot h_i \cdot \left(\frac{h_i}{h_b} \right)^{0.5} \cdot (1.85 \cdot \alpha)^2 \cdot \left(\frac{k_i}{k_{max}} \right)^{0.4} \quad (9)$$

With : $\theta_4 = \pi + \beta$

The specific flow is:

$$\rho_w \cdot g \cdot q = \rho_w \cdot g \cdot \varepsilon \cdot v_c \cdot \sin(\beta) \quad (10)$$

$$= \frac{\Delta p}{\left(\frac{s_1}{k_{max}} \right)} + \frac{\Delta p}{\left(\frac{s_2}{k_{max}} \right)} + \frac{\Delta p}{\left(\frac{s_3}{k_i} \right)} + \frac{\Delta p}{\left(\frac{s_4}{k_i} \right)} = \frac{\Delta p}{R_1} + \frac{\Delta p}{R_2} + \frac{\Delta p}{R_3} + \frac{\Delta p}{R_4} = \frac{\Delta p}{R_t}$$

R1, R2, R3, and R4 are the resistance lines:

$$R_1 = \frac{s_1}{k_{max}} \quad (11)$$

$$R_2 = \frac{s_2}{k_{max}} \quad (12)$$

$$R_3 = \frac{s_3}{k_i} \quad (13)$$

$$R_4 = \frac{s_4}{k_i} \quad (14)$$

The flow line can be into account as parallel resistors and based on the rule of parallel resistors, total resistance is:

$$\frac{1}{R_t} = \frac{1}{R_1} + \frac{1}{R_2} + \frac{1}{R_3} + \frac{1}{R_4} \quad (15)$$

The point pore under pressures in the shear zone and the average pore under pressure are:

$$\Delta p = \rho_w \cdot g \cdot v_c \cdot \varepsilon \cdot \sin(\beta) \cdot R_t \quad (16)$$

$$p_{1m} = \frac{1}{n} \cdot \sum_{i=0}^n \Delta p_i \quad (17)$$

Pore pressure on the blade:

The stream lines at the tip of the blade are:

$$s_1 = \frac{h_b}{\sin(\alpha)} \quad (18)$$

$$s_2 = 0.8 \cdot L_{max} \cdot \theta_2 \quad \text{with : } \theta_2 = \alpha + \beta \quad (19)$$

$$s_3 = 0.8 \cdot L_{max} \cdot \theta_3 \quad \text{with : } \theta_3 = \pi - \beta \quad (20)$$

$$s_4 = 0.9 \cdot h_i \cdot \left(\frac{h_i}{h_b} \right)^{0.5} \cdot (1.85 \cdot \alpha)^2 \cdot \left(\frac{k_i}{k_{max}} \right)^{0.4} \quad (21)$$

R1, R2, R3, and R4 are the resistance lines:

$$R_1 = \frac{s_1}{k_{max}} \quad (22)$$

$$R_2 = \frac{s_2}{k_{max}} \quad (23)$$

$$R_3 = \frac{s_3}{k_i} \quad (24)$$

$$R_4 = \frac{s_4}{k_i} \quad (25)$$

The flow line can be into account as parallel resistors and based on the rule of parallel resistors, total resistance is:

$$\frac{1}{R_t} = \frac{1}{R_1} + \frac{1}{R_2} + \frac{1}{R_3} + \frac{1}{R_4} \quad (26)$$

The point pore under pressures on the blade and the average pore under pressure are:

$$\Delta p = \rho_w \cdot g \cdot v_c \cdot \varepsilon \cdot \sin(\beta) \cdot R_t \quad (27)$$

$$p_{2m} = \frac{1}{n} \cdot \sum_{i=0}^n \Delta p_i \quad (28)$$

The specific energy for the non-cavitating cutting process is:

$$E_{nc} = c_1 \cdot \rho_w \cdot g \cdot v_c \cdot h_i \cdot \frac{\varepsilon}{k_m} \quad (29)$$

Where c1 is:

$$c_1 = \left[\begin{array}{l} \left(\frac{p_{1m} \cdot \frac{\sin(\phi)}{\sin(\beta)} + p_{2m} \cdot \frac{h_b}{h_i} \cdot \frac{\sin(\alpha + \beta + \phi)}{\sin(\alpha)}}{\sin(\alpha + \beta + \delta + \phi)} \right) \cdot \sin(\alpha + \delta) \\ - p_{2m} \cdot \frac{h_b}{h_i} \cdot \frac{\sin(\alpha)}{\sin(\alpha)} \end{array} \right] \cdot \frac{(a_1 \cdot k_i + a_2 \cdot k_{max})}{k_{max}} \quad (30)$$

The specific energy for the cavitating cutting process is:

$$E_{ca} = d_1 \cdot \rho_w \cdot g \cdot (z + 10) \quad (31)$$

Where d1 is:

$$d_1 = \frac{\left(\frac{\sin(\phi)}{\sin(\beta)} + \frac{h_b}{h_i} \cdot \frac{\sin(\alpha + \beta + \phi)}{\sin(\alpha)} \right) \cdot \sin(\alpha + \delta)}{\sin(\alpha + \beta + \delta + \phi)} - \frac{h_b}{h_i} \cdot \frac{\sin(\alpha)}{\sin(\alpha)} \quad (32)$$

Based on the results of the specific energy, it can be determined if the process is cavitating or non-cavitating. If the cutting process is non-cavitating, the following formula applies:

$$W_1 = \frac{p_{1m} \cdot \rho_w \cdot g \cdot v_c \cdot g \cdot h_i^2 \cdot w}{k_{max} \cdot \sin(\beta)} \quad (33)$$

And

$$W_2 = \frac{p_{2m} \cdot \rho_w \cdot g \cdot v_c \cdot g \cdot h_i \cdot h_b \cdot w}{k_{max} \cdot \sin(\alpha)} \quad (34)$$

If the cutting process is cavitating, then:

$$W_1 = \frac{\rho_w \cdot g \cdot (z + 10) \cdot h_i \cdot w}{\sin(\beta)} \quad (35)$$

And

$$W_2 = \frac{\rho_w \cdot g \cdot (z + 10) \cdot h_b \cdot w}{\sin(\alpha)} \quad (36)$$

The above mentioned formulas, are valid when the cutting velocity and the cutting edge are perpendicular. Meaning the blade is moving the longitudinal direction, and therefore, should be represented in a 2D manner. However, when the cutter head is rotating, the angle and the velocity is constantly changing along the different teeth that are mounted of the cutter head. For instance, the velocity of the teeth at the bottom of the head (near the hub) is the highest and the lowest at the top (near the back ring), sometimes so low it can be zero.

Thus, when the blades of a cutter head are divided into small elements, the two-dimensional cutting process should be considered. However, this should be done only if the cutting edge of the element is perpendicular to the element's velocity. The cutting process has many variable parameters, one of these parameters is the rotation of the blade sideways. Meaning that the cutting edge and the velocity of the element at the end of the blade can be regarded as deviations from the original velocity. This velocity consists of two components; a component perpendicular to the cutting edge, and a component parallel to the cutting edge. The friction between the blade and the soil forces it to develop a deviation force on the element. This force, which is known as the snow plough effect, can also cause the soil to move transversely. The equilibrium equations of force have to be calculated in 3D in order to predict the direction of the soil's movement and the blade's deviation force (S. Miedema, 2015).

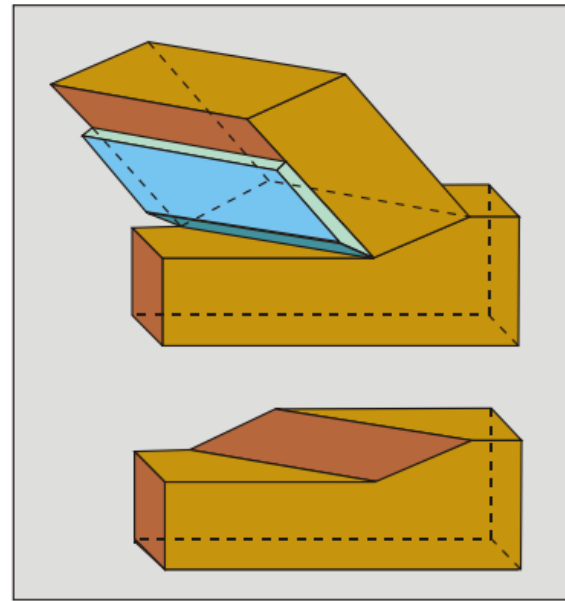


Figure 11, 3D cutting process (S. Miedema, 2015)

The blade's deviation force is not taken into account in this project. Due to time restriction, only the gravitational force, the centrifugal force, and the inertial force of the wedge of soil on top of the blade, are taken into account.

As such, (S. Miedema, 2010) states that water saturated sand should be cohesionless, regardless of the fact that some literature mention that when the condition is water under pressure, it is called apparent cohesion. In this case, the shear stress still follows the rules of Coulomb friction. As a result, the pore volume increases due to the dilatation. The shear plane's under pressure can also develop a strong increase in the grain stresses. As a result, the forces are mainly composed of dilatancy. As such, gravitation, inertia, adhesion and cohesion can be neglected. However, in this project, the effect of the teeth/blade movement is required. Therefore, the gravitational force, centrifugal force, and inertial force are evaluated and their effect on the cutting process of saturated sand is analysed.

Gravitational force:

Gravitational force is the force that is created in consequence of the weight of the wedge of soil that is placed on the blade.

$$F_g = \text{mass} * \text{Gravity} * \cos(\alpha) \quad (37)$$

Centrifugal force:

Centrifugal force is the force that is the result of the rotation of the cutter head. The centrifugal force is calculated by the following formula:

$$F_c = \text{mass} * (\text{cutting speed})^2 / \text{radius of the cutter head} \quad (38)$$

Inertial force:

Inertial force is a consequence of the acceleration of the soil. The inertial force is calculated by the following formula (S. Miedema, 2015):

$$I = \rho_s \cdot v_c^2 \cdot \frac{\sin(\alpha)}{\sin(\alpha + \beta)} \cdot h_i \cdot w \quad (39)$$

Requirements and Pre-conditions

To limit the scope of this project and maintain a specific standard, a set of requirements and boundary conditions are set. The requirements of the MATLAB module are stated to ensure that the final script is running with out any issues and compatible with the other tools that are used at Damen (for example, the kinetic MATLAB module). In addition, the boundary conditions are made to essentially state the limitations that the design of MATLAB and this project cannot surpass.

Requirements for the MATLAB module:

- Use of the version MATLAB 2020.
- The script should not require more than 2 seconds to run.
- The number of loops should be reduced as much as possible, and should be avoided if possible.
- The code should be original to avoid copy right issues.
- A module with clear interface should be created. It should be possible that the module can be used for multiple applications and not for a specific program only.
- The input parameters should be feasible.
- The output results of the cutting forces should be realistic.
- There must not be an empty code or an invalid formula that could results, for example, in a number to be divided by zero.

Pre-conditions:

- The module is made for sand specifically, as it behaves differently that other types of soils. Namely, sand does not have cohesion between the particles and no adhesion.
- Large blade angles should be excluded as they produce a situation that results in a wedge of sand in front of the blade.
- The sand should be in a normal saturated environment.
- It should be considered if the situation is cavitating or non-cavitating.
- The water depth should not be more than 60 meters because in larger depths the casing of the shaft will be experiencing high pressures and could fail.
- No current forces should be considered. Calm conditions are assumed.
- No inclinations which the cutting blade is cutting the soil, as this will results in onset bank collapse because of the permeability and dilatancy.
- The MATLAB module that will be created and the existing MATLAB script should have a one way coupling. Namely, from the existing kinetic MATLAB module to the new module that will be created.

Methodology

Desk research:

To establish the knowledge required to create the MATLAB module and conduct the parameters' defining experiments, research is needed. In addition, desk research is necessitated for the curved trajectories and the dynamic effects of cutting. Furthermore, a description of the basic structure of the cutting tool, the required interaction, and the interface design is essential for obtaining a good understanding of the MATLAB module. Moreover, a chart of the module framework should be provided. Due to the concurrent development, the module should have its own testing environment to demonstrate reliably the proposed frame work and selecting the appropriate modules.

Creating a model using MATLAB where a function will be defined to be called upon:

A representative set of parameters of the rotary cutting process for a specific instance (specific velocity, blade angle, shear angle, position of the teeth, ...etc.) is obtained from the kinetic MATLAB module. Thereafter, several functions are created to acquire the final cutting forces. These results are verified through an experiment that is conducted in a lab.

Experiment to verify the model:

By a mean of an experiment the MATLAB module is evaluated in regards to the rotary movement of the teeth/blade. Only the most defining component of the module will be checked through the experiment. The experiment is relatively simple, e.g. a "blade" is moved through the soil sample to represent the single unite of the process.



Figure 12, Rotary sand cutting experiment

The movement of the blade is achieved by the weight of the bottles that are hanged from a cantilever beam. There are four bottles that have a volume of 1.1 litre and filled with water.

When the weight is let go the blade starts moving through the saturated sand that is places in the bucket.

To acquire results from the experiment. The movement of the blade was filmed in a stationary camera to capture the transition of the blade, frame by frame. Each value obtained from the frames are placed in an excel sheet to be able to calculate the speed,

the acceleration, and the torque that is resulted from the weight of the bottles and the forces that are applied on the blade.

In addition to the above mentioned methods, there are more tests that should be conducted to analyse the soil sample and provide the parameters needed for the cutting forces equations. These tests are more of an analysis supporting the scale test rather than tests themselves. These examinations are:

Sieve analysis:

The soil sample is placed in a tray (weighed beforehand) and spread evenly. It is then inserted in a preheated oven to ensure the soil sample is completely dry. Thereafter, the sample is weighed and noted down. The materials are dumped into a sieve stack for fine materials. The mesh size is ordered in a descending order from the top sieve to bottom sieve. After the sample is sieved for a few minutes, the particles that are left at each sieve will be weighed. The weighed values are then entered into an excel sheet that eventually gives the soil distribution curve and precise values of the diameter of the particle and the percentage finer than D.



Figure 13, Sieve stack

Density test:



Figure 14, Density test

An oven dried soil sample is poured into a metal mould which is weighted first and the dimensions (diameter and height) are noted down to calculate the volume. The soil is poured into the mould using a funnel. Over filling the mould is necessary so that the mould is not shaken, to level the extra soil. A spatula is then used to level the soil surface up to the brim. This way, it is ensured the soil sample is at its loosest state. The mould is then weighed again and noted down. The soil then is removed from the metal mould and the sleeve of the mould is attached. The soil is then filled again up to the sleeve brim and a surcharge load is added on top of the soil. Afterwards, the surcharge load is hammered a number of times until compaction is ensured. The sleeve is removed and the level of the soil is levelled again using a spatula. Then, the sample is weighed one final time and from all the obtained values the relative density can be calculated.

Permeability test:

First, the soil sample is wetted. Then a graduated cylinder with five holes at the bottom is lined with cotton to prevent the soil particles from trickling out of the cylinder. A measured quantity of water is poured on top of the soil sample. Immediately, when the water is poured, a stop watch is set to time how long it took the water to trickle out of the graduated cylinder. Every time the water quantity inside the measured cylinder is reduced 100 ml, the stop watch is stopped and the number of seconds is observed.

In order to establish good results of the permeability, two tests were conducted; one has a level of 42cm sand in the cylinder while the other has 21 cm of sand. In addition to the tests, several permeability equations were used to find the permeability values. The lowest permeability value from the tests and the equations is assumed to be the initial permeability when the soil is at its densest state. Whereas the highest permeability value is assumed to the maximum permeability when the soil sample is at its loosest density. Lastly, the average of all the permeability values is considered to be the effective permeability.

The following equation gives the permeability from the tests:

$$k = 2.3 \frac{aL}{At} \log \frac{h_1}{h_2} \quad (40)$$

As for the equations, several formulas were used from (S. Miedema, 2015) in which the conditions apply to sand sample.

The first equation:

Hazen's equation is used when the soil sample is uniformly graded, the type of soil is in the range from fine sand to gravel, and the effective particle size is 0.1 mm – 3 mm.

$$k = 6 \cdot 10^{-4} \cdot \frac{g}{v_1} \cdot (1 + 10 \cdot (n - 0.26)) \cdot d_{10}^2 \quad (41)$$

The second equation:

Kozney-Carman equation is used when the type of soil is in the range from fine silt to coarse sand, and the flow is a laminar flow.

$$k = 8.3 \cdot 10^{-3} \cdot \frac{g}{v_1} \cdot \frac{n^3}{(1-n)^2} \cdot d_{10}^2 \quad (42)$$

The third equation:

Breyer equation is used when the soil is poorly graded with uniformity coefficient from 1-20, and the effective particles sizes range from 0.06 to 0.6 m.

$$k = 6 \cdot 10^{-4} \cdot \frac{g}{v_1} \cdot \log\left(\frac{500}{U}\right) \cdot d_{10}^2 \quad (43)$$

The fourth equation:

Slitcher equation is used when the soil particle size ranges from 0.01 – 5 mm.

$$k = 1 \cdot 10^{-2} \cdot \frac{g}{v_1} \cdot n^{3.287} \cdot d_{10}^2 \quad (44)$$

Angle of repose test:

To determine the angle of internal friction and the angle of external friction, it is important to know the angle of repose. Therefore, three repose angle tests are conducted to determine the angle of repose and the density of the sample. If the density of the sample coincide with values in the range between 1300-1600 kg/m³ then the angle of repose from the test is valid.

The sand sample is poured slowly onto a flat circular surface (lid of a container), in which the diameter is measured (Figure 15Figure 15).



Figure 15, Measurement of the lid surface

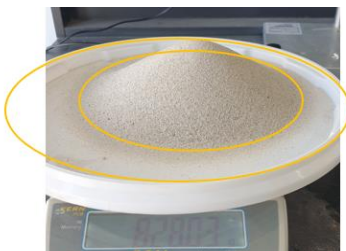


Figure 16, placing ovals in PowerPoint to know the scaling factor

Through using PowerPoint, the scaled size of the ovals (Figure 16) is known, meaning the diameter of the base circle created by the sand sample is known as well.

Next, a rectangle is placed on top of the measuring tape; From PowerPoint the sizes of the base and height of the rectangle are known. Therefore, the scaling factor is known. Therefore, the rotation of the straight lines is also known. And as such the angle of repose is obtained.

Then the density is calculated for each of the tests to make sure that the density values corresponding with the repose angle are feasible.



Figure 17, Using PowerPoint to find the scaling factor

Results

In this chapter, the results of the experiments will be provided and explained. Along with explaining the structure of the MATLAB module and the final outcome of the normal force that is acting on the blade, which takes into account the gravitational, centrifugal, and inertial forces. Later on a comparison of the normal force with or without the additional forces (gravitational, centrifugal, and inertial forces) is given. At last, the results of the soil cutting experiment is presented.

Parameter defining experiments results:

Sieve analysis:

From the sieve analysis and the particle size distribution curve (can be seen in Figure 18), it is established that the sand sample is uniformly graded. Furthermore, the majority of the sand particles' sizes are on the finer side, from 0.2 - 0.3 mm. Additionally, $d_{50} = 0.278$ mm, meaning, 50% of the sand sample has a particle size diameter of less 0.278 mm. Moreover, $d_{10} = 0.184$ mm, and $d_{60} = 0.295$ mm, both of these values are used to determine the permeability of the sample.

Naam:	0	Karakteristieke Korrel Grootten		DAMEN
Projectnr.	A210782	µm	mm	
Samplenr:	0	D10	184 0,184	
Locatie:	0	D15	197 0,197	
Materiaal:	0	D30	243 0,243	
Dn 50:	0,278	D50	278 0,278	
Datum:	23-2-2022	D60	295 0,295	Coefficient van Uniformiteit Cu (D60/D10) 1,60
Aangeleverd door	MvtV	D85	341 0,341	Slibfractie 0,01 % (<0,063mm)
Meting door	MvtV	D90	351 0,351	

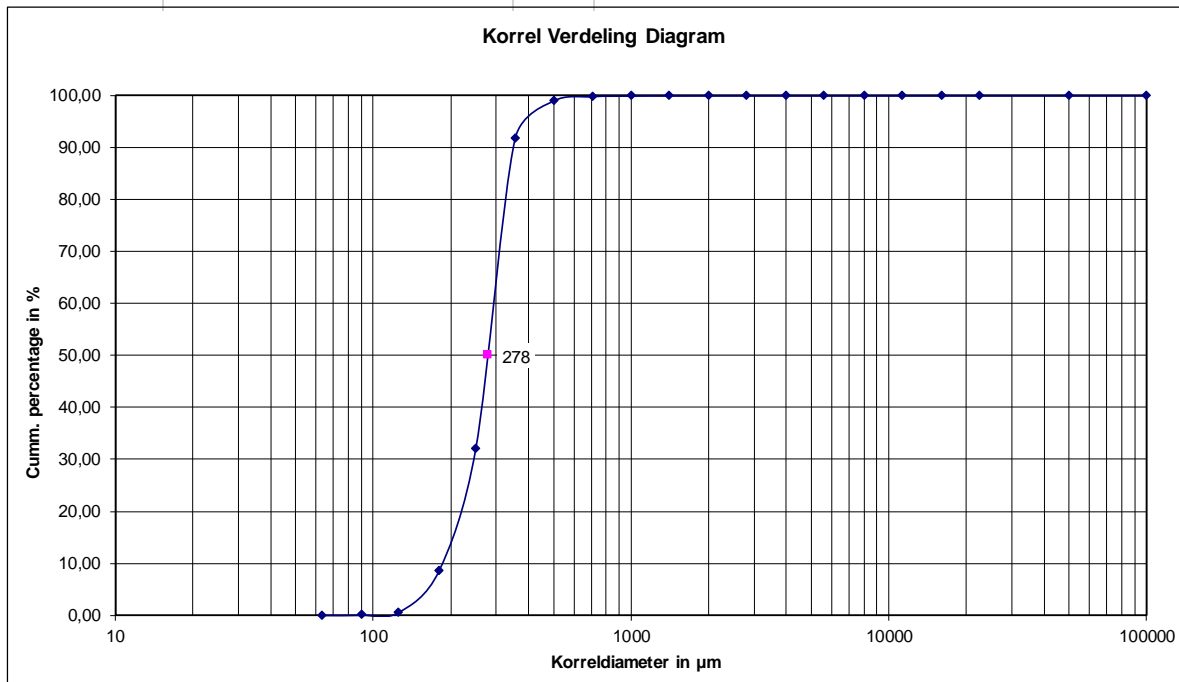


Figure 18, particle size distribution curve obtained from the sieve analysis.

Density test:

For a step by step calculation of the density test please refer to Appendix B. However, the results of the density test are as follows:

$$\rho_{min} = \frac{weight_{loose} - weight_m}{Volume} = 1361.4 \text{ kg/m}^3$$

$$\rho_{max} = \frac{weight_{dense} - weight_m}{Volume} = 1638.5 \text{ kg/m}^3$$

Permeability test:

From Figure 19, the lowest permeability value is the one obtained from the first test. Thus, the initial permeability is $k = 1.59 \times 10^{-5} \text{ m/s}$. In contrast, the highest value of the permeability is attained from Kozeny-Carman formula. In turn, the maximum permeability is $k = 7.8 \times 10^{-4} \text{ m/s}$. Lastly, the effective permeability is assumed to be the average of all the permeability values, regardless if they were acquired from tests or formulas. As such, effective permeability is $k = 3.73 \times 10^{-4} \text{ m/s}$.

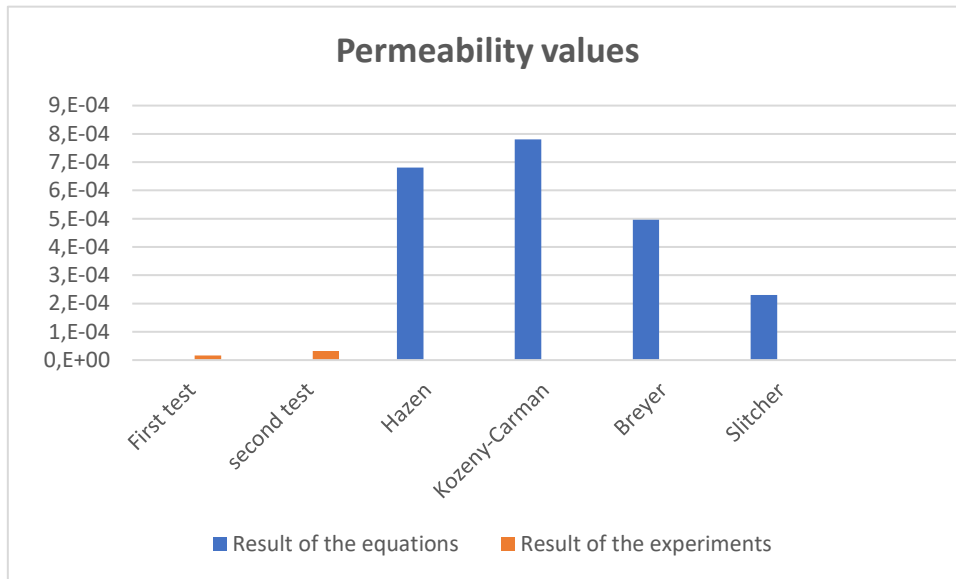


Figure 19, Permeability values from tests and experiments.

Angle of repose test:

For the full step-by-step calculation process, please refer to Appendix D.

Results of the three angle of repose experiments are as follows:

Test number	Angle of repose (degrees)	Density of the sample (kg/m ³)
Test 1	30	1848.7
Test 2	28	1696
Test 3	27.7	1723

Table 2, Angle of repose tests' values

From Table 2, it can be seen that from the first test and third test, the angle of repose values are not valid, due to the densities' high values. The densities of the those tests are not lying in the range from 1300-1600 kg/m³. Hence, only the angle of repose of the second test will be taken into account, even though the density result does not conform with the range. However, it is the lowest density out of all the other tests and therefore, assumed to be the decisive value. In addition, throughout all the tests, the angle of repose is not varying largely, regardless of the big difference of the densities values. As such, the angle of repose is 28°.

MATLAB module results:

In this section, the structure of the MATLAB module is explained (the full final script can be found in Appendix E). In addition, the results of the MATLAB module are discussed.

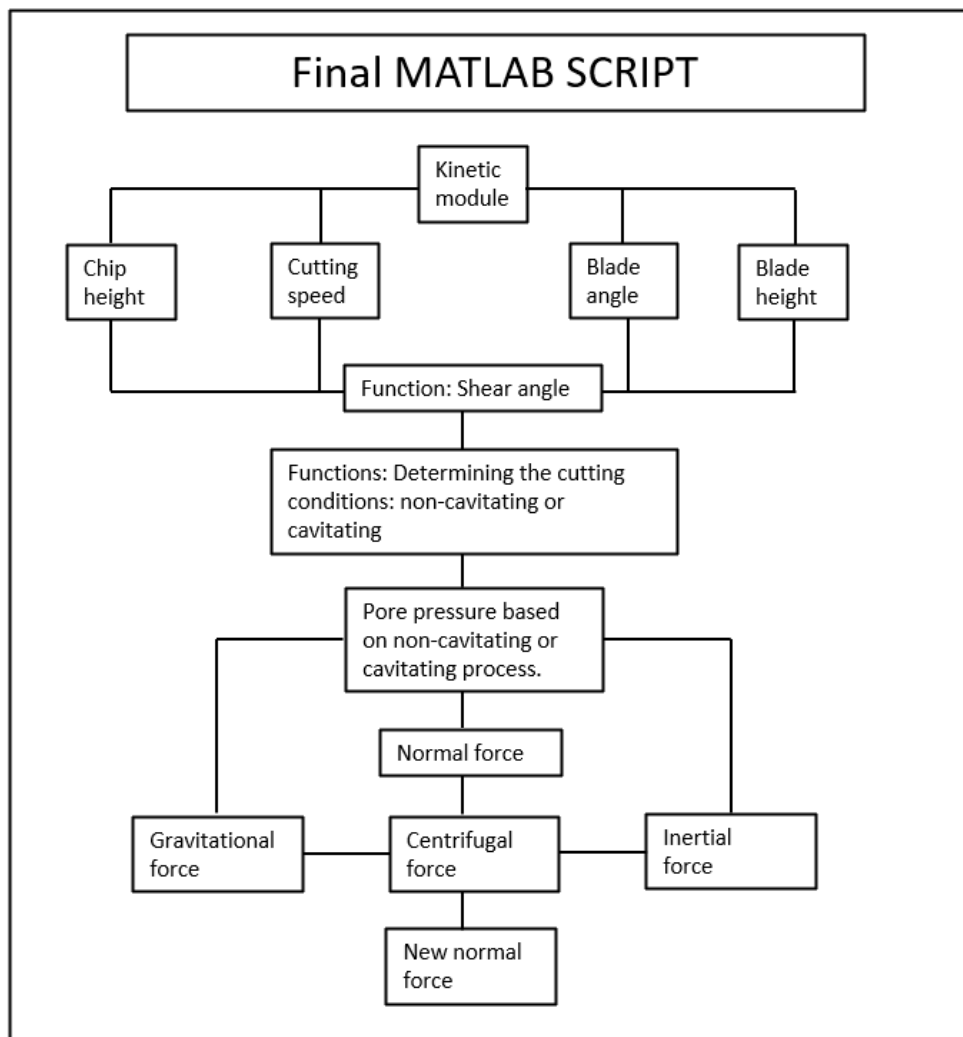


Figure 20, Structure of the MATLAB script

- In order to begin with scripting the module to find the normal force acting on the blade, a few parameters are extracted from the kinetic module to establish starting points.
 - As such the angle of internal friction is assumed to be equal to the angle of repose = 28° .
 - The angle of external friction = 20° according to Table 1, the sand will interact with the steel of the cutting blade.
 - Chip height, cutting speed, blade angle, and blade height are all information extracted from the kinetic teeth movement module (can be seen at the initialization of the code in Appendix E).
- As for the shear angle calculation, formula (3) is used. Therefore, due to the initial height of the cut (h_i) starts at 0 and low values, the second term of the formula is a significantly a large number and thus the shear angle is relatively high. Therefore, a limitation is proposed to limit the values of the shear angle. However, that limitation is a result of trying different formula combinations and succeeding. As such, it is not scientifically proven and in turn has an uncertain validity.

- After the shear angle is determined, several functions were made to establish whether the cutting process is non-cavitating or cavitating. For this, the method (S. Miedema, 2015) proposed to determine the pore pressure in analytical way is utilized (can be seen in the determination of the pore pressure section in Appendix E). After running the script, it was found that the cutting process is a cavitating one. Subsequently, formulas (35) and (36) are used.
- Therefore, the normal force can be calculated using equation (5).

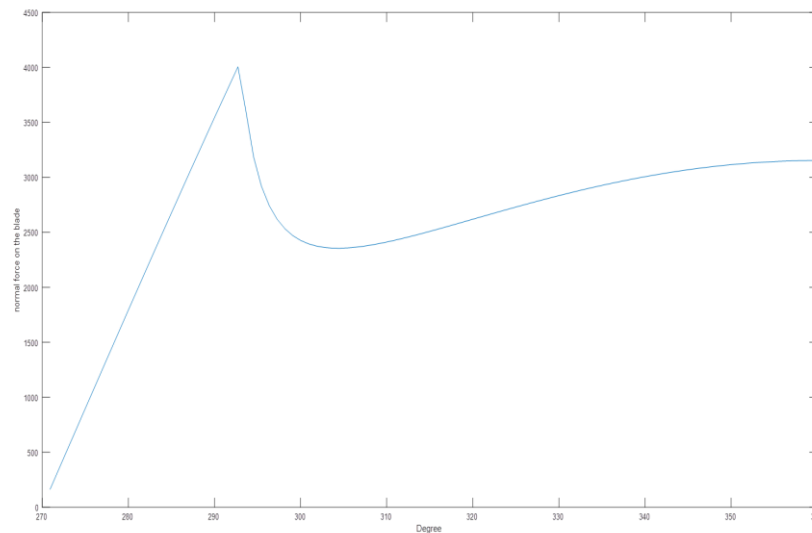


Figure 21, The original normal force

From Figure 21, the normal force value drastically increase along the blade rotation of 20°. Afterwards, the force drops and continue to along an grow to expected values.

However, this sudden upsurge and drop of the force causes the cutter suction dredger's shaft to stutter and could result in damaging the cutting equipment.

- As a result of the rotary movement of the blade while cutting the soil, a number of forces start to effect the total load applied on the blade. Three forces are taken into account, namely, the gravitational force, the centrifugal force, and the inertial force.

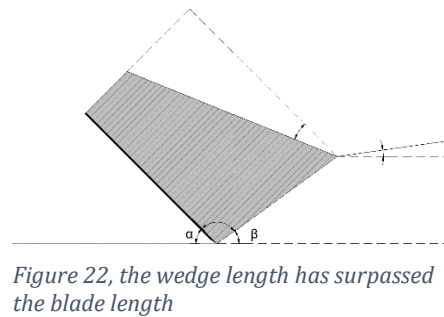
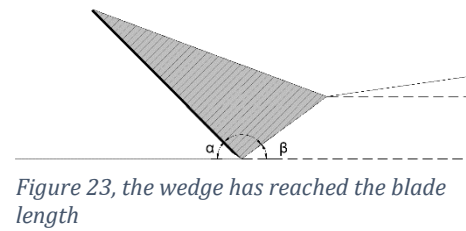
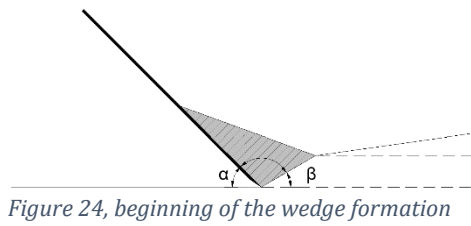
Gravitational force:

To calculate the gravitation force the mass of the soil needs to be known and it is a fairly easy calculations (can be seen below). However, the mass of the wedge is constantly changing over the rotational trajectory of the blade.



- When the blade is cutting the soil, a small quantity of sand is being cut. Accordingly, a small triangle starts to form as a result of the shear length increment over time. Therefore, the area of the wedge is the area of the triangle. However, when the triangle of sand has travelled until the top of the triangle is reached or passed the full blade length, the extra length that is not supported by the blade will fall. Meaning, the area of the wedge in this

case is equal to the four cornered shape (**Error! Reference source not found.**) minus the area of the triangle.



- To define the new normal force a function was created. In the function, the formula (5) is used, in addition to the values of the gravitational force, the centrifugal force and the inertial force calculated by formula (37), (38), and (39) respectively.

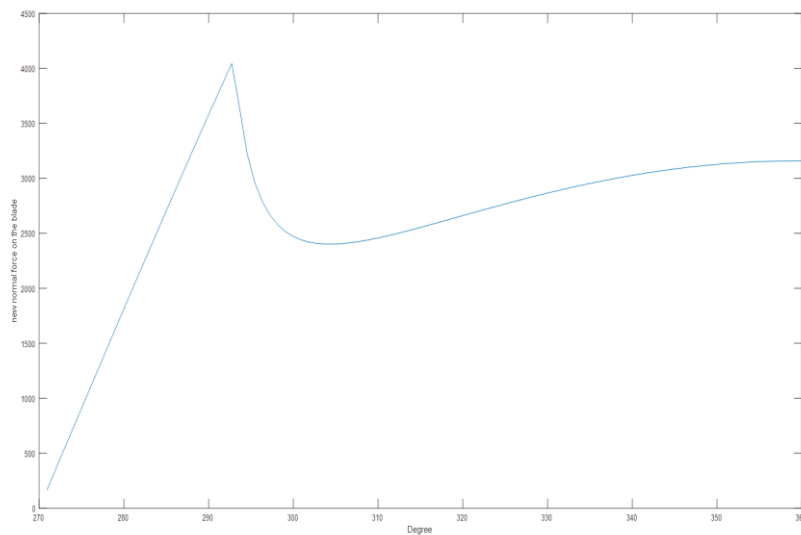


Figure 25, The improved normal forces, with the addition of the gravitational force, the centrifugal force, and the inertial force.

From Figure 25, it is established that the addition of the forces (gravitational, centrifugal, and inertial) only contribute to a small increase of the normal force.

Soil cutting experiment results

The detailed results of the experiment can be found in Appendix F.

After conducting the experiment and filming it, the video is evaluated frame by frame. First the angles of cutting, the cutting speed, and the acceleration are calculated. From then, the torque caused by the cantilever is calculated.

The time it took the blade to cut the soil, the angles from the rotary cutting, and the cutting speed values are used as an input in the MATLAB module. As such, the normal forces on the blade can be compared with the torque of the cantilever.

Results of the normal forces, the original and the improved normal forces are as follows:

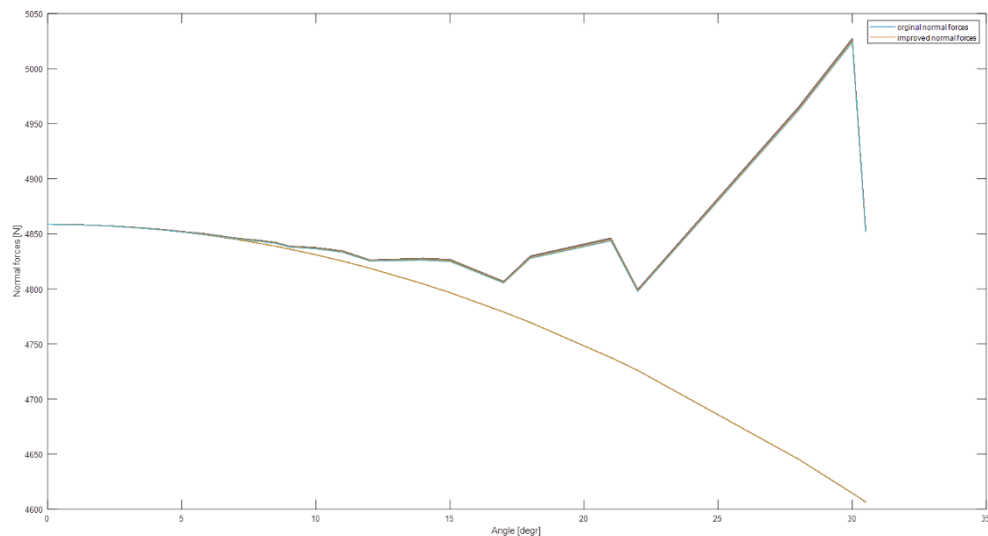


Figure 26, the original and improved normal forces

Since the original normal force formula (5) does not contain the velocity parameter, the graph is a smooth curve. Noticeably, there is approximately 200 N difference between the old and the new normal forces, which is due to the considerable contribution of the gravitational force, inertial force, and the centrifugal force.

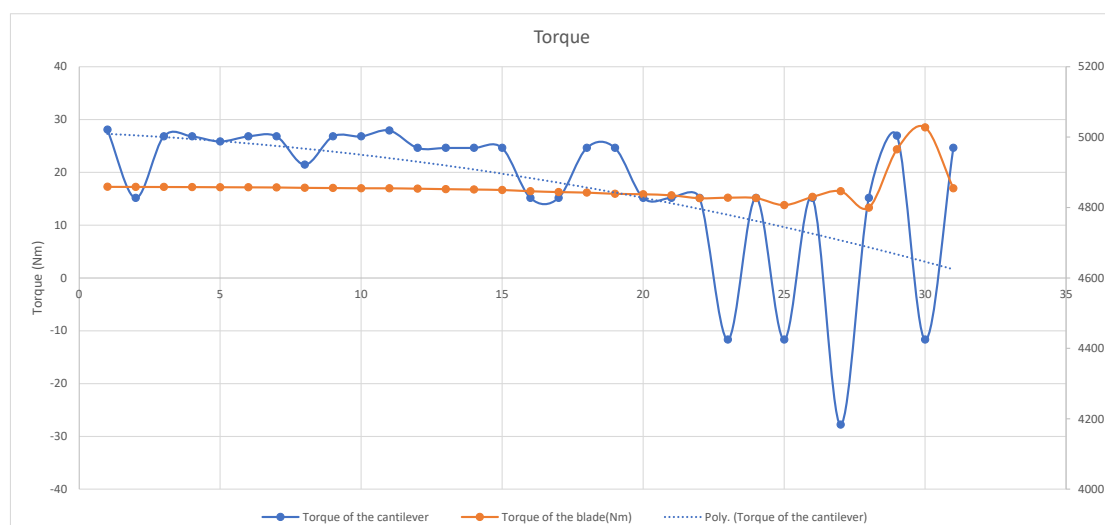


Figure 27, Torque from the forces on the blade (orange) and from the weight of the bottles (blue)

The blue graph is the torque from the bottles (the cantilever beam) is related to the torque from the blade. As can be seen by Figure 27 the scales for each torque is different. The results of the torque on the blade (orange graph) are in alignment with the values of the improved normal forces in Figure 26.

Discussion

In general, the trends from the MATLAB module and the experiment are logical. The MATLAB module is structured in a way that Damen can use the module for different projects. In addition, the module have potential to be expanded with more sub-scripts to evolve from the 2D to the 3D cutting theory.

However, there are some results that need further elaboration and qualification of the end values. These are evaluated one by one.

The average pore pressure on the blade:

There are some improvements to be made of the MATLAB module. For instance, when creating the script, the average pore pressure on the blade and the shear zone was based on the analytical method (S. Miedema, 2015) has proposed. However, he states that the method depends in soil mechanics parameters which are not very accurate and therefore should be used as a first estimate.

The original and improved normal forces values:

- Appendix G, shows the ratio of between the values of the normal forces at each moment in time. The average ratio is = 0.8%, which is relatively low. This signifies that the additional forces; namely, gravitational, centrifugal, and inertial forces, are do not have a large influence on the cutting process. It can be concluded that, (S. Miedema, 2015) is correct in his assumption that the centrifugal forces, gravitational forces, and inertial forces can be neglected as a result, the pore volume increases due to the dilatation which is confirmed from the MATLAB module.
- Furthermore, the graphs of both Figure 21 and Figure 25 show a stuttering behaviour of the normal force, meaning, a sudden surge followed by an immediate drop. This is an undesirable effect, as it can damage the shaft and causes the teeth and the arms of the cutter head break more often.

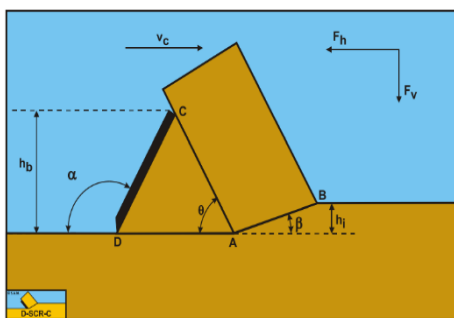


Figure 28, cutting sand with a wedge

- The sudden increase and drop in the force is created because of the wedge phenomena, which occur when the blade angle is relatively high. For instance, when the shear angle and the blade angle are positioned in a way that the cutting profile contains a wedge in front of the blade that is pushing the soil. When this happens the soil is being cut by the wedge rather than the blade. As such, it required more effort to cut the soil. However, this is beyond the scope of this project, as it requires an in depth analysis. Thus, only the normal force values that are in accordance with 290 degrees and higher are considered in this project.

Soil cutting experiment results:

- In normal dredging circumstances, the increase of the gravitational, centrifugal, and inertial force in Figure 26, is not encountered. That is due to the fact that, normal dredging conditions are usually occurring in the left area of the graph in accordance with 0-approximately 12 degrees, and there the contribution is quite low.
- From figure 26, the shape of the graphs are what is expected. However, there is factor of 100 between the difference of the results from the experiment and the MATLAB module. This is an indication that there is a multiplication in the MATLAB module by 100. This will be checked in the future.
- From the experiment it is not expected that real quantitative values can be obtained. However, a confirmation that the values of the cutting forces and the velocities obtained from the MATLAB module are feasible. Meaning, the dynamic aspect of the soil cutting is confirmed through the experiment. For example, the trend of the improved normal forces values matches with the trend from the experiment values of the torque.

Conclusion and recommendations

Ultimately, this research accomplishes its objective to supply DAMEN with a modular program to showcase the soil cutting processes. The MATLAB module will be used along with further research to optimize the results even further. In addition, Damen would like to develop similar tools for other type of soil, e.g. clay, rock, and dry sand to obtain the forces applied on the teeth of the cutter head. Although, the soil other than sand display a complete different behaviour and properties, this MATLAB module can still be used as template for the other programs.

The MATLAB module is not going to be used for engineering purposes because from the results, it is established that there is a small increment of the normal force acting on the blade. However, this increment of the normal force is negligible for engineering purposes. On the other hand, the MATLAB script is going to be used by Damen in the future for the calculation of the forces applied on the blade.

Based on the MATLAB module it is shown that the increment of the new normal force does not exceed more than 1% and therefore can be considered negligible. However, this is due to the dilatation effect on the shear zone.

From the soil cutting experiment, it is established that when in fields conditions the forces of the old and new normal forces are similar. However, when the soil is cut in different conditions then the effect the rotary cutting movement of the soil starts to become more noticeable.

All in all, through the creation of the MATLAB module the main research question **What is the relation between the movement of cutter head's teeth of the CSD through the sediment and effort it takes?** is answered.

Recommendations:

- Due to the time limit, the permeability result could have been improved further by conducting several test for different conditions, such as when the soil sample is at its densest or loosest state.

- Information about dredging and soil cutting is relatively limited and therefore many assumptions are defined to obtain results that are feasible. As such, there are some uncertainties, thus, further research is needed.
- Again, due to the short period of time available, the effect the snow plough phenomena would have had on the blade/teeth in regards to load increments were not taken into account. In addition, although 3D cutting theory would have provided more accurate results, only 2D cutting theory was considered to simplify the processes and results.
- To limit the results of the shear angle to reasonable values, a limitation was implemented. However, the limitation was based on trying different values and equations until one emerged. As such, it is not scientifically proven and in turn has an uncertain validity.
- The shear line or the failure line is considered a straight line when in reality the line is part of a curve or more curvy than straight. Therefore, that is something to be considered for the future to optimize the cutting process.

References

Association of Dredging Companies, I. (n.d.). *INTERNATIONAL ASSOCIATION OF DREDGING COMPANIES*.

Budhu, M. (2010). *Soil mechanics and foundations* (3rd ed.). Library of Congress Cataloging-in-Publication Data.

Damen Dredging Equipment - Damen. (n.d.). Retrieved March 21, 2022, from <https://www.damen.com/companies/damen-dredging-equipment>

DEME takes delivery of 'Spartacus' - the most powerful and innovative cutter suction dredger in the world | DEME Group. (n.d.). Retrieved March 21, 2022, from <https://www.deme-group.com/news/deme-takes-delivery-spartacus-most-powerful-and-innovative-cutter-suction-dredger-world>

DREDGING HISTORY. (n.d.). Retrieved March 21, 2022, from <http://www.alldredgeholland.com/>

Miedema, S.A., (1987), "Calculation of the Cutting Forces when Cutting Water Saturated Sand".

Miedema, SA. (2010). New developments of cutting theories with respect to offshore applications. In JS. Chung, R. Ayer, S. Prinsenber, SW. Hong, & I. Langen (Eds.), *The proceedings of the twentieth* (2010)

Miedema, SA. (2015). *The Delft Sand, Clay & Rock Cutting Model. Family Edition*. (3 ed.) IOS Press.

Miedema, S.A., "On the Snow-Plough Effect when Cutting Water Saturated Sand with Inclined Straight Blades".ASCE Proc. Dredging 94, Orlando, Florida, USA, November 1994.

Purushothama, P. (2013). *Soil mechanics and foundation engineering* (2nd ed.). Dorling Kindersley (India) Pvt. Ltd. .

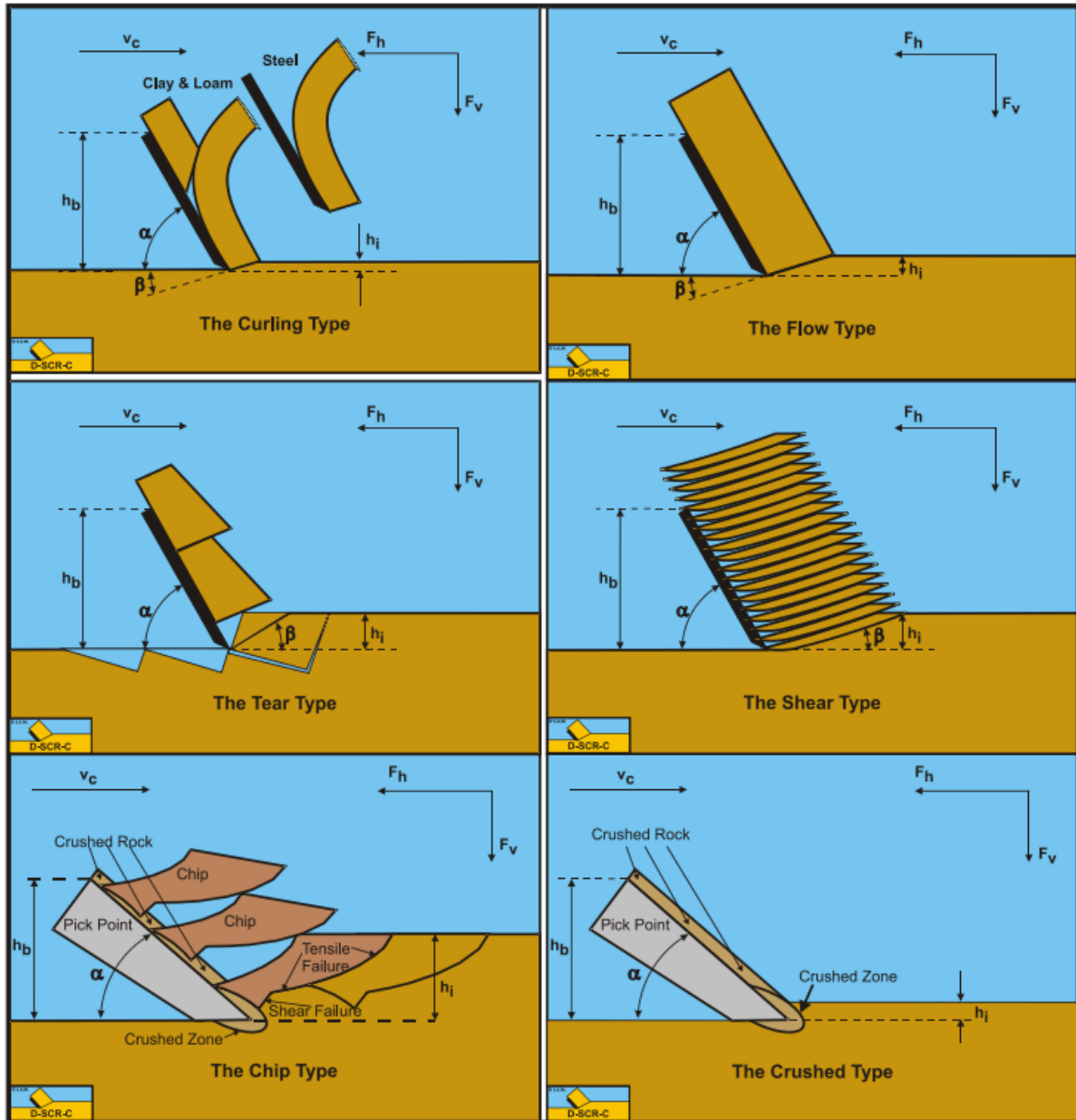
Verruit, A; 2001; Grondmechanica; Dictaat Grondmechanica; TU Delft, Delft, the Netherlands

- Arnold Verruijt, *An Introduction to Soil Mechanics*, Springer International Publishing AG 2018, 2018
- Vlasblom, W. J. (2005). *Designing Dredging Equipment Wb 3408b*. TU Delft
- VOUW. (2010a). *Grondmechanica (Vol. 1)*. Vereniging van waterbouwers in Bagger-, Kust- en Oeverwerken te Leidschendam
- VOUW. (2010b). *Snijkopzuiger (Vol. 5a)*. Vereniging van waterbouwers in Bagger-, Kust- en Oeverwerken te Leidschendam
- VOUW. (2010b). *Snijkopzuiger (Vol. 5a)*. Vereniging van waterbouwers in Bagger-, Kust- en Oeverwerken te Leidschendam
- VOUW. (2010c). *Use of equipment and production estimate (Vol. 10)*. Vereniging van waterbouwers in Bagger-, Kust- en Oeverwerken te Leidschendam
- Wankhede, A. (n.d.). *What is Dredging - History, Importance And Effects*. Retrieved March 21, 2022, from <https://www.marineinsight.com/guidelines/what-is-dredging/>
- What is dredging?* (n.d.). Retrieved March 21, 2022, from <https://oceanservice.noaa.gov/facts/dredging.html>
- Why start dredging? - Start Dredging*. (n.d.). Retrieved March 21, 2022, from <https://startdredging.com/why-dredge/>
- Winkelman, M. (n.d.). *Which Teeth Will Survive The Cut? Adapting Your Selection – Discover Dredging*. Retrieved March 21, 2022, from <https://www.discoverdredging.com/which-teeth-will-survive-the-cut-adapting-your-selection/>
- Yasheng, M., Fusheng, N., & Miedema, S. (2006). *Calculation of the Blade Cutting Force for small Cutting Angles based on MATLAB*. Conference: The 2nd China Dredging Association International Conference & Exhibition, themed 'Dredging and Sustainable Development' At: Guangzhou, China
- Zhao, Y., & Miedema, S. (2001). *Finite element calculations to determine the pore pressures when cutting water saturated sand at large cutting angles*. In *CEDA Dredging Day*. Conference: CEDA Dredging Days At: Rotterdam, The Netherlands

Appendices

Appendix A

The different types of failure mechanisms that can occur depending the soil types.



Appendix B

First the metal mould is measured and weighed. The dimension of the metal mould are as follows:

height = 35 cm = 0.035 m

diameter = 55 cm = 0.055 m

weight_m = 67.67 g = 0.068 kg

As such, the volume of the mould is $= \frac{\pi(0.055)^2}{4} * 0.035 = 8.3 * 10^{-5} m^3$

Then the soil is poured loosely and the mould is weighed again.

$$\text{weight}_{\text{loose}} = 180.96 \text{ g} = 0.181 \text{ kg}$$

$$\rho_{\text{min}} = \frac{\text{weight}_{\text{loose}} - \text{weight}_m}{\text{Volume}} = 1361.4 \text{ kg/m}^3$$

After, the soil is compacted into the metal mould and weight on final time.

$$\text{Weight}_{\text{dense}} = 180.96 \text{ g} = 0.181 \text{ kg}$$

$$\rho_{\text{max}} = \frac{\text{weight}_{\text{dense}} - \text{weight}_m}{\text{Volume}} = 1638.5 \text{ kg/m}^3$$

Appendix C

The first permeability test with soil height of 42 cm in the cylinder:

The time it took for the water level to drop from 600 ml to 500 ml in the graduated cylinder is, $t = 480 \text{ s}$

While $L = 0.042 \text{ m}$

$$h_1 = 600 \text{ ml} / 10^6 = 0.0006 \text{ m}^3$$

$$h_2 = 500 \text{ ml} / 10^6 = 0.0005 \text{ m}^3$$

$A = a =$ area of the graduate cylinder, therefore:

$$k = 2.3 \frac{a L}{A t} \log \frac{h_1}{h_2} = 2.3 \frac{l}{t} \log \frac{h_1}{h_2} = 1.59 * 10^{-5} \text{ m/s}$$

The second permeability test with soil height of 21 cm in the cylinder:

The time it took for the water level to drop from 600 ml to 500 ml in the graduated cylinder is, $t = 120 \text{ s}$

While $L = 0.021 \text{ m}$

$$h_1 = 600 \text{ ml} / 10^6 = 0.0006 \text{ m}^3$$

$$h_2 = 500 \text{ ml} / 10^6 = 0.0005 \text{ m}^3$$

$A = a =$ area of the graduate cylinder, therefore:

$$k = 2.3 \frac{a L}{A t} \log \frac{h_1}{h_2} = 2.3 \frac{l}{t} \log \frac{h_1}{h_2} = 3.19 * 10^{-5} \text{ m/s}$$

As for the equations, several formulas were used from (S. Miedema, 2015) in which the conditions apply to sand sample.

The first equation:

Hazen's equation is used when the soil sample is uniformly graded, the type of soil is in the range from fine sand to gravel, and the effective particle size is 0.1 mm – 3 mm.

$$k = 6 \cdot 10^{-4} \cdot \frac{g}{v_1} \cdot (1 + 10 \cdot (n - 0.26)) \cdot d_{10}^2$$

Where (v_1) the kinematic viscosity is $v_1 = \frac{\mu_1}{\rho_1}$

$$\mu_1 = 0.0010016 \text{ pa*s}$$

$$\rho_1 = 1000 \text{ kg/m}^3$$

$$v_1 = 10^{-6} \text{ m}^2/\text{s}$$

$$\text{And } n = 0.255(1 + 0.83^U)$$

U in the previous formula is the coefficient of grain uniformity $U = \frac{d_{60}}{d_{10}} = \frac{0.295}{0.184} = 1.6$

$$n = 0.255(1 + 0.83^{1.6}) = 0.44$$

$$k = 6 * 10^{-4} \frac{g}{v_1} (1 + 10(n - 0.26)) d_{10}^2 = 6 * 10^{-4} \frac{9.81}{10^{-6}} (1 + 10(0.44 - 0.26)) 0.184^2 = 6.81 * 10^{-4} \text{ m/s}$$

The second equation:

Kozney-Carman equation is used when the type of soil is in the range from fine silt to coarse sand, and the flow is a laminar flow.

$$k = 8.3 * 10^{-3} \cdot \frac{g}{v_1} \cdot \frac{n^3}{(1-n)^2} \cdot d_{10}^2$$

$$k = 8.3 * 10^{-3} \frac{g}{v_1} \left(\frac{n^3}{(1-n)^2} \right) d_{10}^2 = 8.3 * 10^{-3} \frac{9.81}{10^{-6}} \frac{0.44^3}{(1-0.44)^2} 0.184^2 = 7.8 * 10^{-4} \text{ m/s}$$

The third equation:

Breyer equation is used when the soil is poorly graded with uniformity coefficient from 1-20, and the effective particles sizes range from 0.06 to 0.6 m. Since U = 1.6 in the sample used for the project and the effective grain size is 0.184 mm, the use of Breyer formula is valid.

$$k = 6 * 10^{-4} \cdot \frac{g}{v_1} \cdot \log \left(\frac{500}{U} \right) \cdot d_{10}^2$$

$$k = 6 * 10^{-4} \frac{g}{v_1} \log \left(\frac{500}{U} \right) d_{10}^2 = 6 * 10^{-4} \frac{9.81}{10^{-6}} \log \left(\frac{500}{1.6} \right) 0.184^2 = 4.96 * 10^{-4} \text{ m/s}$$

The fourth equation:

Slitcher equation is used when the soil particle size ranges from 0.01 – 5 mm.

$$k = 1 * 10^{-2} \cdot \frac{g}{v_1} \cdot n^{3.287} \cdot d_{10}^2$$

$$k = 1 * 10^{-2} \frac{g}{v_1} n^{3.287} d_{10}^2 = 1 * 10^{-2} \frac{9.81}{10^{-6}} 0.44^{3.287} 0.184^2 = 2.3 * 10^{-4} \text{ m/s}$$

Appendix D

First test:

The sand sample is poured slowly onto a flat circular surface (lid of a container), in which the diameter is measured

Lid diameter = 0.27 m

Through using PowerPoint, the scaled size of the ovals is known, meaning the diameter of the base circle created by the sand sample is known as well.



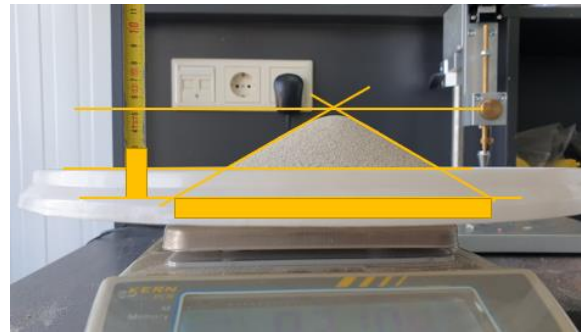
From PowerPoint:

Lid oval;	h = 0.0532 m
	w = 0.1248 m
Base oval;	h = 0.0376 m
	w = 0.0814 m

As such, base oval diameter = lid diameter * $W_{\text{base oval}}/W_{\text{lid oval}} = 0.27 * 0.0814 / 0.1248 = 0.176$ m

The mass of the sample is also known; mass = 0.828 kg.

Next, a rectangle is placed on top of the measuring tape; tape length = 0.03 m. From PowerPoint the sizes of the base and height of the rectangle are known. Therefore, the scaling factor is known.



Tape rectangle;	h = 0.0146 m
	w = 0.0058 m

Base rectangle;	h = 0.0053 m
	w = 0.0906 m

Hence, base rectangle diameter = $W_{\text{base rectangle}} * \text{tape length} / W_{\text{tape rectangle}} = 0.0906 * 0.03 / 0.0058 = 0.186$ m

Base average diameter = base rectangle diameter * base oval diameter / 2 = $0.186 * 0.176 / 2 = 0.181$ m

Base surface = $0.25 * \pi * \text{Base average diameter}^2 = 0.25 * \pi * 0.181^2 = 0.0257$ m²

The measurement from the bottom of the measuring tape to the top horizontal line is; top measurement = 0.054 m.

The left line length from PowerPoint is;

Line 1 L;	h = 0.034 m
	w = 0.0601 m

The angle of repose1 = $\text{atan}(h/w) = 0.5148$ rad = 29.49°

The right line length from PowerPoint is;



Line 1 R; $h = 0.0305 \text{ m}$
 $w = 0.0529 \text{ m}$

The angle of repose2 = $\text{atan}(h/w) = 0.523 \text{ rad} = 29.9^\circ$

Top calculated = base oval diameter* $(\sin(\text{angle of repose1})\sin(\text{angle of repose2}))/\sin(\text{angle of repose1}+\text{angle of repose2})$
 = $0.176*(\sin(0.5148)*\sin(0.523))/\sin(0.5148+0.523) = 0.0503 \text{ m}$

Top average = top measured + top calculated / 2 = $0.054+0.0503/2 = 0.052 \text{ m}$

Volume cone = top average*base surface/3 = $0.052*0.0257/3 = 0.000448 \text{ m}^3$

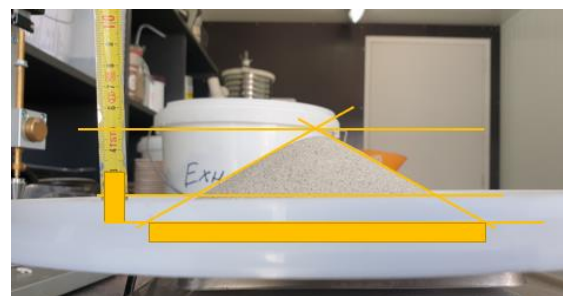
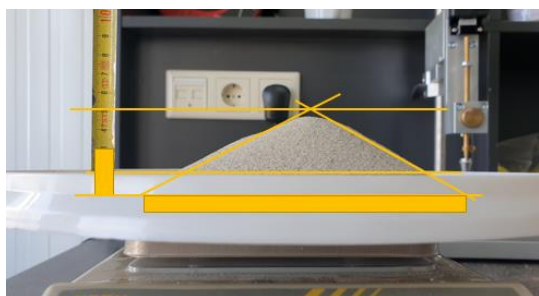
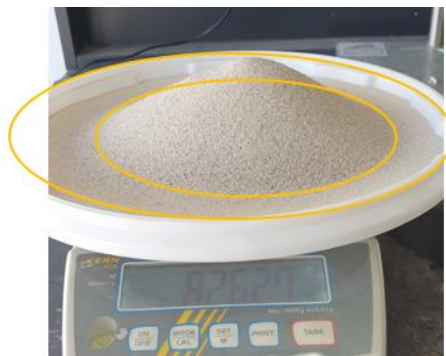
Denisty = mass/volume = $0.828/0.000448 = 1848.7 \text{ kg/m}^3$

However, the density value is rather large. As a result, the values of the repose angle are not feasible.

Second test:

The same process of the previous test applied for the second and the third tests. However, two added pictures are taken to show the repose angle from different views (rotated 90°) in the second and third test.

Therefore, as to not repeat the extensive explanation of the method and the results, only the results is provided now.



Part 1

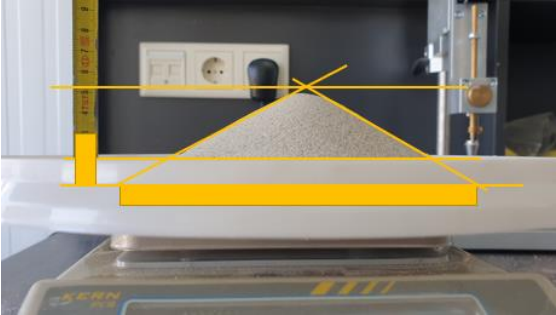
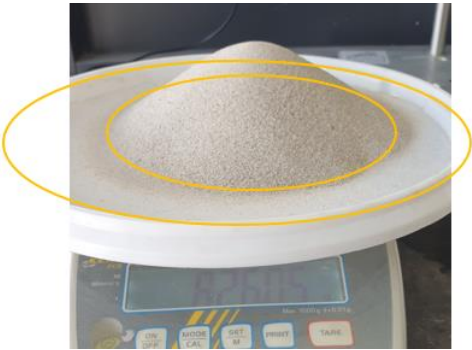
Mass		826,27 gr	0,82627 kg
Lid oval	h	4,47 cm	0,0447 m
	w	11,99 cm	0,1199 m
Base oval	h	3,12 cm	0,0312 m
	w	8,12 cm	0,0812 m
Base oval diameter		18,28524 cm	0,182852 m
Tape rectangle	h	1,46 cm	0,0146 m
	w	0,58 cm	0,0058 m
Base rectangle	h	0,53 cm	0,0053 m
	w	9,99 cm	0,0999 m
Base rectangle diameter		20,5274 cm	0,205274 m
Base average diameter		19,40632 cm	0,194063 m
Base surface		2,95785 cm	0,029578 m
Top measured 1		5,2 cm	0,052 m
Line 1 L	h	3,18 cm	0,0318 m
	w	6,28 cm	0,0628 m
	a	26,85626 °	0,46873 rad
Line 1 R	h	3,1 cm	0,031 m
	w	5,6 cm	0,056 m
	a	28,96766 °	0,505581 rad
Top calculated 1		4,835709 cm	0,048357 m
Top average		5,017854 cm	0,050179 m
Volume cone		494,7353 cm ³	0,000495 m ³
Density		1,670125 ton/m ³	1670,125 kg/m ³

Part 2

Mass		826,27 gr	0,82627 kg
Lid oval	h	4,47 cm	0,0447 m
	w	11,99 cm	0,1199 m
Base oval	h	3,12 cm	0,0312 m
	w	8,12 cm	0,0812 m
Base oval diameter		18,28524 cm	0,182852 m
Tape rectangle	h	1,46 cm	0,0146 m
	w	0,58 cm	0,0058 m
Base rectangle	h	0,53 cm	0,0053 m
	w	9,67 cm	0,0967 m
Base rectangle diameter		19,86986 cm	0,198699 m
Base average diameter		19,07755 cm	0,190776 m
Base surface		2,85848 cm	0,028585 m
Top measured 2		5 cm	0,05 m
Line 2 L	h	3,47 cm	0,0347 m
	w	6,25 cm	0,0625 m
	a	29,03903 °	0,506827 rad
Line 2 R	h	3,15 cm	0,0315 m
	w	5,69 cm	0,0569 m
	a	28,96904 °	0,505605 rad
Top calculated 2		5,06867 cm	0,050687 m
Top average		5,034335 cm	0,050343 m
Volume cone		479,6848 cm ³	0,00048 m ³
Density		1,722527 ton/m ³	1722,527 kg/m ³

Average denisty 1696,326 kg/m³

Third test:



Part 1

Mass		826,05 gr	0,82605 kg
Lid oval	h	4,63 cm	0,0463 m
	w	13,12 cm	0,1312 m
Base oval	h	3,2 cm	0,032 m
	w	8,12 cm	0,0812 m
Base oval diameter		16,71037 cm	0,167104 m
Tape rectangle	h	1,46 cm	0,0146 m
	w	0,58 cm	0,0058 m
Base rectangle	h	0,53 cm	0,0053 m
	w	9,99 cm	0,0999 m
Base rectangle diameter		20,5274 cm	0,205274 m
Base average diameter		18,61888 cm	0,186189 m
Base surface		2,722683 cm	0,027227 m
Top measured 1		5,25 cm	0,0525 m
Line 1 L	h	3,34 cm	0,0334 m
	w	6,44 cm	0,0644 m
	a	27,41277 °	0,478443 rad
Line 1 R	h	3,12 cm	0,0312 m
	w	5,46 cm	0,0546 m
	a	29,74488 °	0,519146 rad
Top calculated 1		4,543152 cm	0,045432 m
Top average		4,896576 cm	0,048966 m
Volume cone		444,3941 cm ³	0,000444 m ³
Density		1,858823 ton/m ³	1858,823 kg/m ³

Part 2

Mass		826,05 gr	0,82605 kg
Lid oval	h	4,63 cm	0,0463 m
	w	13,12 cm	0,1312 m
Base oval	h	3,2 cm	0,032 m
	w	8,12 cm	0,0812 m
Base oval diameter		16,71037 cm	0,167104 m
Tape rectangle	h	1,46 cm	0,0146 m
	w	0,58 cm	0,0058 m
Base rectangle	h	0,53 cm	0,0053 m
	w	11,68 cm	0,1168 m
Base rectangle diameter		24 cm	0,24 m
Base average diameter		20,35518 cm	0,203552 m
Base surface		3,254167 cm	0,032542 m
Top measured 2		5,2 cm	0,052 m
Line 2 L	h	3,44 cm	0,0344 m
	w	6,52 cm	0,0652 m
	a	27,81646 °	0,485489 rad
Line 2 R	h	3,48 cm	0,0348 m
	w	6,64 cm	0,0664 m
	a	27,65887 °	0,482738 rad
Top calculated 2		4,39354 cm	0,043935 m
Top average		4,79677 cm	0,047968 m
Volume cone		520,3164 cm ³	0,00052 m ³
Density		1,587592 ton/m ³	1587,592 kg/m ³
Average denisty		1723,207 kg/m ³	

Appendix E

```
clear
clc
clf
close all

angleFriction = atan(0.4);
angleIntFriction = 28*pi/180;

radiusCutter = 1.8/2;
angleTips = [ 270*pi/180 - 0;
              270*pi/180 - (360/5)*pi/180 ];
angleArmTip = 55*pi/180;
lengthBlade = 100/1000;

depthWorking = 12;
rotCutter = 2*pi*32/60;
speedSwing = 15/60;

timeRange = linspace(0,120,120+1)';

lengthPitch = speedSwing*2*pi/rotCutter/5;
paramOper = [rotCutter speedSwing];
speedTan = rotCutter * radiusCutter;

% demo chip height
heightChip = lengthPitch * cos(linspace(pi*3/2,2*pi)');
plot(linspace(pi*3/2,2*pi)*180/pi,heightChip);
xlabel('Degree'), ylabel('chip height');

% demo cutting speed
speedCut = speedSwing*ones(100,1) - speedTan*sin(linspace(pi*3/2,2*pi)');
figure
plot(linspace(pi*3/2,2*pi)*180/pi,speedCut);
xlabel('Degree'), ylabel('cutting speed');

% demo blade angle
angleBlade = angleArmTip*ones(100,1) - (pi/2-1*atan(speedTan/speedSwing))*...
            cos(linspace(pi*3/2,2*pi)');
figure
plot(linspace(pi*3/2,2*pi)*180/pi,angleBlade*180/pi);
xlabel('Degree'), ylabel('blade angle');

% demo height blade
heightBlade = lengthBlade * sin(angleBlade);
figure
plot(linspace(pi*3/2,2*pi)*180/pi,heightBlade);
xlabel('Degree'), ylabel('height blade');

% demo shear angle
angleShear = shear_angle(heightBlade,heightChip,angleBlade,angleFriction,...
                          angleIntFriction);
angleShear(1) = nan;
figure
```

```
plot(linspace(pi*3/2,2*pi)*180/pi,angleShear*180/pi);
xlabel('Degree'), ylabel('shear angle');

%{
Determining what is the pore pressure based on if the cutting process is
cavitating or non-cavitating
%}

%Constants
permInitial = 1.59e-5;
permMax = 7.8e-4;
GRAV_ACC = 9.81;
RHO_W = 1000;
dilat = 1.2;
widthBlade = 55/1000;

%average pore pressure on the shear plane
angleTeta1 = Teta_1(angleBlade, angleShear);
angleTeta2 = Teta_2(angleBlade, angleShear);
angleTeta3 = Teta_3(angleShear);
angleTeta4 = Teta_4(angleShear);
Lmax = lengthShear_max(heightChip, angleShear);
L1 = 100/1000;
L4 = length_4(heightChip, heightBlade, angleShear, permInitial, permMax);
L = lengthVariable(Lmax);
S1 = lengthStreamLine_1(Lmax, L, angleTeta1, L1,angleBlade);
S2 = lengthStreamLine_2(L, angleTeta2);
S3 = lengthStreamLine_3(L, angleTeta3);
S4 = lengthStreamLine_4(Lmax, L, angleTeta4, L4,angleBlade);
R1 = resistance_1(S1, permMax);
R2 = resistance_2(S2, permMax);
R3 = resistance_3(S3, permInitial);
R4 = resistance_4(S4, permInitial);
Rt = resistanceTotal(R1, R2, R3, R4);
Dp = pressurePore(RHO_W, GRAV_ACC, speedCut, dilat, angleShear, Rt);
P1m = avg_pres_pore_shear(Dp);

% Average pore pressure on the blade
S_1_b = lengthStreamLine_1_b(L1,angleBlade);
S_2_b = lengthStreamLine_2_b(Lmax, angleTeta2);
S_3_b = lengthStreamLine_3_b(Lmax, angleTeta3);
S_4_b = lengthStreamLine_4_b(L4);
R1_b = resistance_1_b(S_1_b, permMax);
R2_b = resistance_2_b(S_2_b, permMax);
R3_b = resistance_3_b(S_3_b, permInitial);
R4_b = resistance_4_b(S_4_b, permInitial);
Rt_b = resistanceTotal(R1_b, R2_b, R3_b, R4_b);
Dp_b = pressurePore_blade(RHO_W, GRAV_ACC, speedCut, dilat, angleShear, Rt_b);
P2m = avg_pres_pore_balde(Dp_b);

%Specific energy for the non-cavitating cutting process
a1 = 0.5;
a2 = 0.5;
```

```

angleExtFriction = 20*pi/180;
permEffect = 3.73e-4;
C1 = coef_non_cav(P1m, angleIntFriction, angleShear, P2m, heightBlade, ...
    heightChip, angleBlade, angleExtFriction, a1, a2, permMax, permInitial);
Enc = enrgy_non_cav(C1, RHO_W, GRAV_ACC, speedCut, dilat, heightChip, permEffect);

%Specific energy for the cavitating cutting process
d1 = coef_cav_1(angleIntFriction, angleShear, heightBlade, heightChip, ...
    angleBlade, angleExtFriction);
Eca = enrgy_cav(d1, RHO_W, GRAV_ACC, depthWorking);
if Enc<Eca
    disp('W1 and W2 are based on the non-cavitating process')

else
    disp('W1 and W2 are based on the cavitating process')
end

% normal force on blade
pressShear = W_P_shear_cav(RHO_W, GRAV_ACC, depthWorking, heightChip, ...
    widthBlade, angleShear);
pressBlade = W_P_blade_cav(RHO_W, GRAV_ACC, depthWorking, heightChip, ...
    widthBlade, angleBlade);
forceNormalBlade = N_F_blade(pressShear,pressBlade,angleFriction, ...
    angleBlade,angleShear,angleIntFriction);
figure
plot(linspace(pi*3/2,2*pi)*180/pi,forceNormalBlade);
xlabel('Degree'), ylabel('normal force on the blade');
arrayCheck = [linspace(pi*3/2,2*pi)' angleBlade angleShear ...
    (angleBlade+angleShear+angleIntFriction+angleFriction)] *180/pi;

% mass of the soil wedge on the blade
RHO_LOOSE = 1361.4;
timeCut = linspace(pi*3/2,2*pi)'./rotCutter'-1.4;
m = mass(radiusCutter, rotCutter,angleShear,angleBlade,heightChip,dilat, ...
    speedCut,timeCut,lengthBlade,widthBlade,RHO_LOOSE);
m(1) = 0;

% Gravitaional force
Fg = forceGrav(m, GRAV_ACC, angleBlade);

% Centrifugal force
Fc = forceCentrifugal(m,speedCut,speedTan,radiusCutter);

% Intertia force
RHO_S = 1650;
Fi = forceInertia(RHO_S, speedCut, angleBlade, angleShear, heightChip, widthBlade);

% normal force on the blade with all the additional forces
N_blade_all_f = N_F_blade_all_f(pressShear, pressBlade, angleFriction, angleBlade,
angleShear, angleIntFriction, Fg, Fc, Fi);
figure
plot(linspace(pi*3/2,2*pi)*180/pi,N_blade_all_f);

```

```
xlabel('Degree'), ylabel('new normal force on the blade');
```

```
% Comparison between the old and the new normal force
```

```
forceNormalBlade(1)=0;
```

```
N_blade_all_f(1)=0;
```

```
ratio = 100-forceNormalBlade./ N_blade_all_f.*100;
```

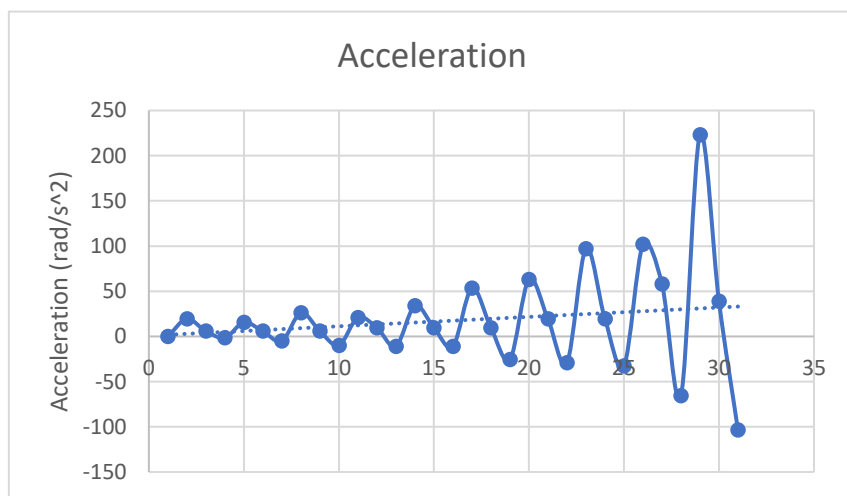
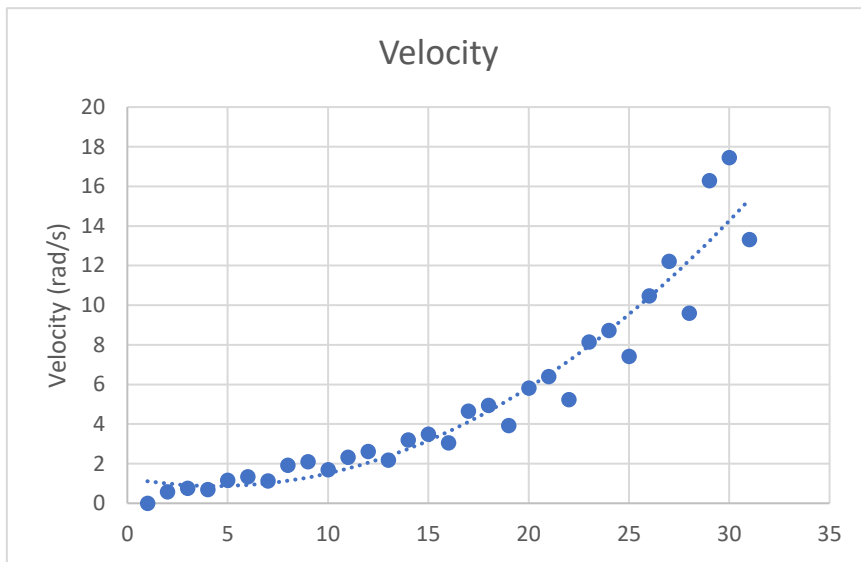
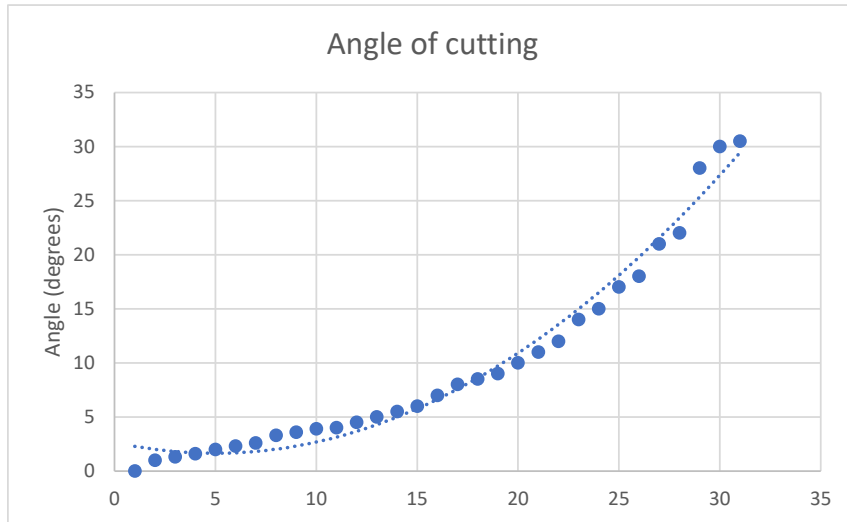
```
ratio(1) = 0;
```

```
disp(table(forceNormalBlade, N_blade_all_f, ratio, 'VariableNames', {'old normal force', 'new normal force', 'ratio (%)'}))
```

Appendix F

N	Time coordinates	Registered angle	Rotation angle (degree)	Rotation angle (rad)	Speed (rad/s)	Acceleration (rad/s ²)
1	0	6	0	0	0	0
2	0,03	7	1	0,017453293	0,581776417	19,39254724
3	0,06	7,3	1,3	0,02268928	0,756309343	5,817764173
4	0,1	7,6	1,6	0,027925268	0,698131701	-1,454441043
5	0,13	8	2	0,034906585	1,163552835	15,5140378
6	0,16	8,3	2,3	0,040142573	1,33808576	5,817764173
7	0,2	8,6	2,6	0,045378561	1,134464014	-5,090543652
8	0,23	9,3	3,3	0,057595865	1,919862177	26,17993878
9	0,26	9,6	3,6	0,062831853	2,094395102	5,817764173
10	0,3	9,9	3,9	0,068067841	1,701696021	-9,817477042
11	0,33	10	4	0,06981317	2,327105669	20,84698829
12	0,36	10,5	4,5	0,078539816	2,617993878	9,696273622
13	0,4	11	5	0,087266463	2,181661565	-10,90830782
14	0,43	11,5	5,5	0,095993109	3,199770295	33,93695768
15	0,46	12	6	0,104719755	3,490658504	9,696273622
16	0,5	13	7	0,122173048	3,054326191	-10,90830782
17	0,53	14	8	0,13962634	4,654211339	53,32950492
18	0,56	14,5	8,5	0,148352986	4,945099547	9,696273622
19	0,6	15	9	0,157079633	3,926990817	-25,45271826
20	0,63	16	10	0,174532925	5,817764173	63,02577854
21	0,66	17	11	0,191986218	6,399540591	19,39254724
22	0,7	18	12	0,20943951	5,235987756	-29,08882087
23	0,73	20	14	0,244346095	8,144869843	96,96273622
24	0,76	21	15	0,261799388	8,72664626	19,39254724
25	0,8	23	17	0,296705973	7,417649321	-32,72492347
26	0,83	24	18	0,314159265	10,47197551	101,810873
27	0,86	27	21	0,366519143	12,21730476	58,17764173
28	0,9	28	22	0,383972435	9,599310886	-65,44984695
29	0,93	34	28	0,488692191	16,28973969	223,0142933
30	0,96	36	30	0,523598776	17,45329252	38,78509449
31	1	36,5	30,5	0,532325422	13,30813555	-103,6289243

Length (m)	applied force (N)	Torque of the cantilever (Nm)	Length of the pendulum (m)	Normal force applied on the blade (N)	Torque of the blade(Nm)	Total torque (Nm)
0,65	43,164	28,0566	0,8	48,58669636	0	28,0566
0,65	43,164	15,15904567	0,8	48,58401574	32,70563166	-17,54658598
0,65	43,164	26,80349374	0,8	48,58217354	37,44940078	-10,64590704
0,65	43,164	26,80349374	0,8	48,57978516	38,84725671	-12,04376297
0,65	43,164	25,84183988	0,8	48,57604704	35,33605967	-9,494219782
0,65	43,164	26,80349374	0,8	48,57265297	28,97670439	-2,173210651
0,65	43,164	26,80349374	0,8	48,56854233	20,02972016	6,773773583
0,65	43,164	21,45887131	0,8	48,55814407	-6,127870514	27,58674183
0,65	43,164	26,80349374	0,8	48,55287335	-17,18851123	43,99200497
0,65	43,164	26,80349374	0,8	48,54627649	-26,7107889	53,51428264
0,65	43,164	27,91643386	0,8	48,54522298	-29,39131671	57,30775057
0,65	43,164	24,62198291	0,8	48,53470717	-37,95531041	62,57729332
0,65	43,164	24,62198291	0,8	48,5210676	-37,22242365	61,84440655
0,65	43,164	24,62198291	0,8	48,51078779	-27,38105361	52,00303652
0,65	43,164	24,62198291	0,8	48,49755592	-10,840775	35,46275791
0,65	43,164	15,15904567	0,8	48,46191927	25,47106521	-10,31201953
0,65	43,164	15,15904567	0,8	48,43852899	38,33844648	-23,17940081
0,65	43,164	24,62198291	0,8	48,42283668	30,93200884	-6,310025934
0,65	43,164	24,62198291	0,8	48,3888512	15,95355205	8,66843086
0,65	43,164	15,15904567	0,8	48,3756731	-21,05390994	36,21295561
0,65	43,164	15,15904567	0,8	48,34568833	-38,67617189	53,83521756
0,65	43,164	15,15904567	0,8	48,26399615	-20,7177226	35,87676827
0,65	43,164	-11,67566533	0,8	48,2779448	38,25958979	-49,93525512
0,65	43,164	15,15904567	0,8	48,26790156	25,11042356	-9,951377888
0,65	43,164	-11,67566533	0,8	48,06877532	-36,97056002	25,29489469
0,65	43,164	15,15904567	0,8	48,29925919	-29,01770214	44,17674782
0,65	43,164	-27,77582348	0,8	48,46202037	32,43681808	-60,21264156
0,65	43,164	15,15904567	0,8	47,99596115	-0,339861677	15,49980735
0,65	43,164	26,93911366	0,8	49,65286937	10,76099978	16,17811389
0,65	43,164	-11,67566533	0,8	50,27293663	-39,73700098	28,06133565
0,65	43,164	24,62198291	0,8	48,54664946	-30,80293606	55,42491896



Appendix G

old normal force	new normal force	ratio (%)
0	0	0
163.4	164.84	0.87254
326.85	329.76	0.88332
490.3	494.68	0.88548
653.71	659.55	0.8852
817.05	824.33	0.8837
980.27	988.99	0.88141
1143.3	1153.5	0.8785
1306.2	1317.7	0.87507
1468.8	1481.7	0.87117
1631.2	1645.4	0.86684
1793.2	1808.8	0.86209
1954.9	1971.8	0.85695
2116.2	2134.3	0.85143
2277	2296.4	0.84554
2437.4	2458	0.83929
2597.2	2619	0.8327
2756.5	2779.5	0.82577
2915.2	2939.3	0.81851
3073.3	3098.4	0.81093
3230.6	3256.8	0.80304
3387.3	3414.4	0.79484
3543.2	3571.3	0.78636
3698.3	3727.3	0.77758
3852.6	3882.4	0.76854
4006	4036.6	0.75923
3608.1	3639.1	0.85352
3185.6	3216.9	0.97326
2920	2951.6	1.0693
2742.7	2774.5	1.1466
2619.8	2651.9	1.2088
2532.9	2565.2	1.2586
2471	2503.5	1.2982
2427	2459.7	1.3291
2396.5	2429.3	1.3528
2376.1	2409.1	1.3703
2363.6	2396.7	1.3823
2357.3	2390.6	1.3898
2356.1	2389.4	1.3931
2358.9	2392.2	1.3929
2365	2398.3	1.3896
2373.8	2407.1	1.3834
2384.8	2418.1	1.3747
2397.7	2430.9	1.3638
2412.2	2445.2	1.3509
2427.9	2460.8	1.3363
2444.7	2477.4	1.32
2462.3	2494.8	1.3023
2480.7	2512.9	1.2832
2499.6	2531.6	1.2631

2519	2550.7	1.2419
2538.8	2570.1	1.2197
2558.8	2589.8	1.1968
2579	2609.6	1.1731
2599.3	2629.5	1.1488
2619.7	2649.5	1.1239
2640.1	2669.4	1.0985
2660.4	2689.2	1.0728
2680.6	2708.9	1.0467
2700.7	2728.5	1.0203
2720.6	2747.9	0.99368
2740.2	2767	0.96692
2759.7	2785.9	0.94006
2778.9	2804.5	0.91315
2797.7	2822.7	0.88624
2816.3	2840.7	0.85938
2834.5	2858.3	0.83261
2852.3	2875.5	0.80598
2869.7	2892.3	0.77954
2886.8	2908.7	0.75332
2903.4	2924.6	0.72735
2919.5	2940.2	0.70169
2935.2	2955.2	0.67637
2950.5	2969.8	0.65141
2965.3	2984	0.62686
2979.5	2997.6	0.60274
2993.3	3010.7	0.5791
3006.5	3023.3	0.55594
3019.3	3035.5	0.53332
3031.5	3047	0.51125
3043.1	3058.1	0.48975
3054.2	3068.6	0.46886
3064.7	3078.5	0.4486
3074.7	3088	0.42898
3084.1	3096.8	0.41004
3092.9	3105.1	0.39179
3101.2	3112.8	0.37426
3108.8	3120	0.35745
3115.9	3126.5	0.34138
3122.3	3132.5	0.32608
3128.2	3137.9	0.31156
3133.4	3142.8	0.29783
3138	3147	0.2849
3142.1	3150.6	0.27278
3145.5	3153.7	0.26149
3148.2	3156.2	0.25103
3150.4	3158	0.24142
3152	3159.3	0.23265
3152.9	3160	0.22474
3153.2	3160.1	0.21769

>>